Nano-structured Ti(CN) based cermets

A DISSERTATION

Submitted in partial fulfilment of the

requirements for the award of the degree

of

INTEGRATED DUAL DEGREE

(Bachelor of Technology & Master of Technology)

in

METALLUGICAL AND MATERIALS ENGINEERING

(With Specialization in Materials Engineering)

By

VIKRANT KESHARI HALDAR

(Enrollment no - 12216020)

DEPARTMENT OF METALLURGICAL AND MATERIALS ENGINEERING

INDIAN INSTITUTE OF TECHNOLOGY, ROORKEE

ROORKEE – 247667 (INDIA)

MAY, 2018

Indian Institute of Technology Roorkee

Roorkee

CANDIDATE'S DECLARATION

I hereby declare and certify that the work which is being presented in the DISSERTATION entitled **"NANO-STRUCTURED Ti(CN) BASED CERMETS"** in partial fulfilment of the requirement for the award of the DEGREE OF MASTER OF TECHNOLOGY with specialization in MATERIALS ENGINEERING submitted in the Departmet of Metallurgical and Materials Engineering of the Indian Institute of Technology Roorkee, Roorkee is an authentic record of my own work carried out during the period from May 2017 to May 2018 under the supervision of DR. B.V. Manoj Kumar, assistant professor, Department of Metallurgical and Materials Engineering, Indian Institute of Technology Roorkee, Roorkee.

The matter presented in this thesis has not been submitted by me for the award of any other degree of this or any other Institute.

Dated: May 2018

Place: Roorkee (VIKRANT KESHARI HALDAR)

CERTIFICATE

This is to certify that the above statement made by the candidate is correct to the best of my knowledge and belief.

DR. B.V. MANOJ KUMAR

Assistant Professor,

MMED, IIT Roorkee

Roorkee- 247667 (India)

ACKNOWLEDGEMENT

I would like to express my gratitude and thanks to my guide Dr. B.V. Manoj Kumar, Assistant Professor, Metallurgical and Materials Engineering Department, Indian Institute of Technology Roorkee, for his valuable guidance, inspiration and generous help in carrying out this work. It would not have been possible to materialize the concepts in the area of **"Nano-structured Ti(CN) based cermets"**, as without his proper guidance completing this project would have been a monumental task. Working under him was a privilege and an excellent chance to learn and grow, which I will cherish for the life time.

I wish to express my sincere thanks to Dr. Anjan Sil, Professor and Head of the Department, Metallurgical and Materials Engineering Department, IIT ROORKEE, for his help to carry out this dissertation.

My heartfelt thanks goes to Mr. Yashpal Sharma and Mr. Nilesh Dorkar, Research Scholar, MMED for their guidance and relentless support and help during the whole work and making me understand portion of work which I was unable to understand.

Special thanks goes to all the lab members and faculty for their help and kind co-operation throughout the course of my project work.

I would like to acknowledge my friends for their valuable information and help, and boosting my morale throughout the work.

Last but not the least, I would like to thank my parents for making me walk this earth and for all they did, after which everything else was possible.

ABSTRACT

The present work deals with the samples prepared with composition TiCN-10wt%WC-10wt%TaC-10wt%Co-10wt%Ni at different sintering parameters to check the change in microstructure and the resulting changes that accompanies with the hardness and fracture toughness. The sintering parameters were changed to achieve a high dense material. The final temperature was kept at 1200℃, 1300℃, 1350℃ and 1500℃. In all cases the holding time was kept at 3 min at the final temperature. The heating rate was kept at 100℃/min for initial samples and 600℃/min for the last three samples. Load applied was 40MPa. SEM images reveals the formation of core-rim structure for the samples. Core consists of undissolved TiCN whereas the rim consist of a solid solution of (Ti,Ta,W)CN. The microstructure was of spheroidal shape due to grain shape accommodation. The Carbide (core+rim) size was the main factor the changes in the mechanical properties of the sintered samples. Hardness and fracture toughness of the samples sintered at 1350℃ and 1500℃ were 10.79GPa, 6.51 MPa√m and 16.11GPa, 7.70 MPa√m. There was a decrease in the carbide (core+rim) size which led to an increase in the mechanical properties and decrease in the wear volume of the sample. The fracture morphology of the sample revealed the presence of mix of two fracture mechanism that is trans-granular fracture and intra-granular grain fracture. The worn out region showed the presence of oxides which was confirmed from FESEM-EDS analysis.

Contents

List of figures

List of Tables

CHAPTER 1 INTRODUCTION

1.1 Growing need in industries

With the advancement of technology in the present world in manufacturing sector machining has become an upmost part of it. So along with advancement there is a huge rush to minimize the cost of production while increasing the production rate at which it is manufactured to favor the economy to one's side. Thus in order to do so machining has been made economical viable and this can be achieved either by reducing the machining time or by reducing non-machining time. The non-machining time can be reduced by automation while machining can be done by increasing machining speed which means that remains an issue to the engineers. This leads to the production of high machining tools which can withstand high temperature and has superior wear resistance.

1.2 Properties requirement for high machining tools

Following properties are supposed to be possessed by a cutting tools:

- Hot hardness: Tools should have proper hot hardness to maintain sharp and consistent cutting edge during high temperature working conditions.
- Toughness: Able to absorb and withstand forces and shock loads produced during machining.
- Thermal shock resistance: Tools must possess high thermal shock resistance so no change in microstructure arises while machining and should not degrade upon cooling or when exposed to sudden changes in temperature.
- Abrasion resistance: Should withstand the change in dimensions if encountered any rubbing effect.
- Chemical stability: should not be any affinity between tools and workpiece.

1.3 Materials used

Usually the composite of ceramics and metals used to make tools consists of Ti(CN) or TiC or TiN along with carbides of Ta, W, Mo, Nb or V. One can either use Ni or Co or Mo as binder phase to bind all this carbides or combination of two. Composites with Al_2O_3, ZrO_2 and Si_3N_4 are used for electro conductive components or for cutting tools**.**

But in our present study, we will focus mainly on the composites of ceramics and metals consisting of Ti(CN) along with other metals carbides like VC, NbC, Mo_2C, WC, TaC.

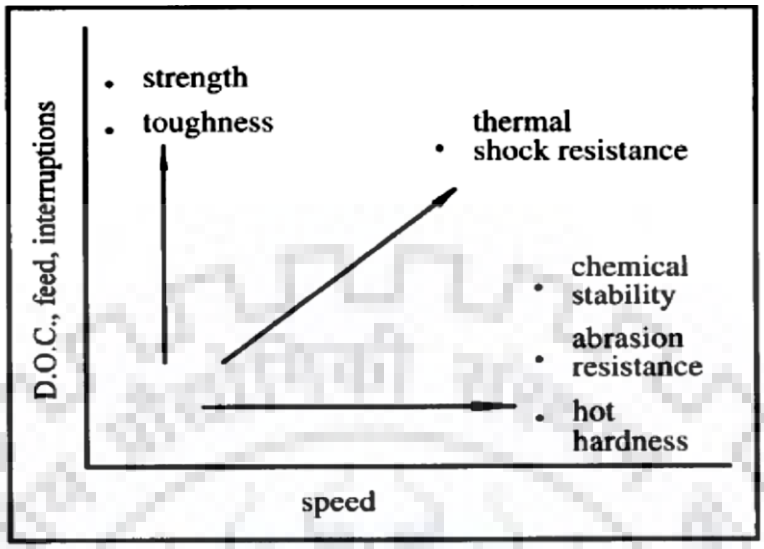

Fig 1.1 Effect of machining parameters on the emphasis on different properties of tool material.

Ti(CN) based ceramics and cermets have heterogeneous and complex composition and microstructure, which usually arises from variety of components used to make it composition, but the metal-binder system are usually Co, Ni, Fe or alloys.[1]. Usually the final composition of the binder depends highly on the stoichiometry, the C/N ratio of the hard phases and solubility of each involved phases during sintering [1].

The microstructures of such cermets are complex because

(i) reactions among the starting components during sintering
(ii) denitrification-decarburization when sintering is under high pressure or high vacuum or in an inert atmosphere
(iii) contamination from milling media or by any external factors.

Solubility of hard phases into the binder is a key factor in promoting strong metal-ceramic bond, which is a requirement from a tool for superior performance. The formation of core-rim structure also inhibits growth and coalescence of the carbo-nitride grains during sintering.

In present work, we have made a sample comprising the composition of TiCN-10wt%WC-10wt%TaC-10wt%Co-10wt%Ni by SPS at different temperatures to attain the suitable relative density. Microstructure and mechanical properties of these materials are studied and discussed.

Further the influence of the microstructural features on the performance in sliding wear conditions is studied.

1.4 Research scope

In recent times there has been a rise in the use of cermets as a material for cutting tool in industries, owing its high suitability as a high speed machining tool material. Thus due to this reason there has been an increase in the studies of ceramic-metal composite, which has been carried out in the last two decades. The scope for introducing a highly suitable cermet has been on the rise. Research on the performance of ultrafine or nano-structured TiCN based cermets has led to an important findings which has confirmed to possess improved physical, mechanical and tribological properties at room temperature and even at higher temperature [3,6].

There are three principle ways of getting ultrafine TiCN cermet till date, i.e. applying nano-sized TiCN powders [40-42], adding nano additives [43-47] into TiCN cermet matrix and sintering it with fast sintering techniques [48-51].

Of all the sintering methods, only five methods are quite popular for preparing ultrafine cermets, namely self-propagating reaction at high temperature synthesis or mechanically sustaining reaction, synthesis by high-temperature solid-state diffusion from TiN-TiC, TiN-C, TiC-Ti powder blends, carbothermic reduction synthesis, mechanical alloying and chemosynthesis. All these methods have their own pros and cons which have been discussed in literature review of this report.

Still there are some hindrance which prevent the commercialization of ultrafine TiCN based cermet, one of which is processing of these powders. Other is leakage that usually arises during sintering. Processing methods which have been developed are very costly and are limited to shapes and sizes only. Another problem is the contamination of nano-sized particles which in turn adversely affects the mechanical properties. Thus keeping all those points in mind the research thrust areas, following issues are dealt in this work:

i. Determining the changes in the microstructure that arises from change in sintering conditions
ii. Understanding the sliding wear characteristics of cermet as related to microstructure.

Objective of the thesis:

Major objective of the thesis are as follows

i. To optimise the sintering operating conditions to achieve fully dense cermets.
ii. To study microstructural and mechanical characteristics of sintered cermets.
iii. To understand the wear mechanisms of the cermets system in the sliding wear conditions

Cermets is ideally designed to have optimum properties of both ceramics and metals i.e. having high temperature resistance and hardness along with the ability to undergo plastic deformation.

2.1 Titanium Carbo-Nitride [Ti(CN)]

It is a non-oxide classed material whose composition is made entirely by a solid solution of TiC and TiN as Ti(CxN1-x) {where x varies from $0 \leq x \leq 1$}.[2]

Ti(CN) has an FCC based structure or rock salt type crystal structure. Two most widely accepted models of Ti(CN)

i. Ti-ordered C–N-disordered FCC NaCl type structure (Fig 1a) in which Ti occupies the (0 0 0), and C and N atoms randomly occupy the (1/2 1/2 1/2) sites.
ii. The $TiC_{0.50}N_{0.50}$ crystal can be described using a tetragonal unit cell (Fig 1b), in which Ti atoms occupy (0 0 0), (1/2 1/2 0), (0 1/2 1/2) and (1/2 0 1/2) sites, N atoms occupy (0 0 1/2) and (1/2 1/2 1/2) sites, and C atoms occupy (0 1/2 0) and (1/2 0 0) sites [35].

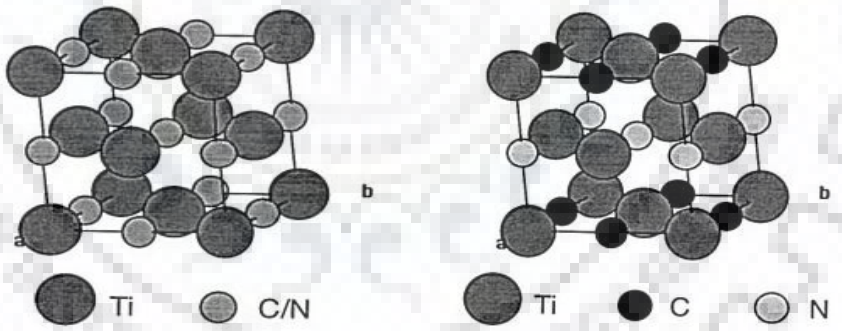

(a) (b)

Fig2.1 Schematic representation of two possible structures of TiCN [35].

2.1.1 Property variation of $TiC_{1-x}N_x$

The properties of Ti(CN) cermets are to a certain degree depend on C/N ratio in the mixture. In studies it has been shown that lattice parameter decreases with increasing N content (Fig 2.2(a)) [5,6]. The Knoop hardness also decreases with increasing N amount (Fig 2.2(b)) whereas toughness shows are completely reverse in nature [7].

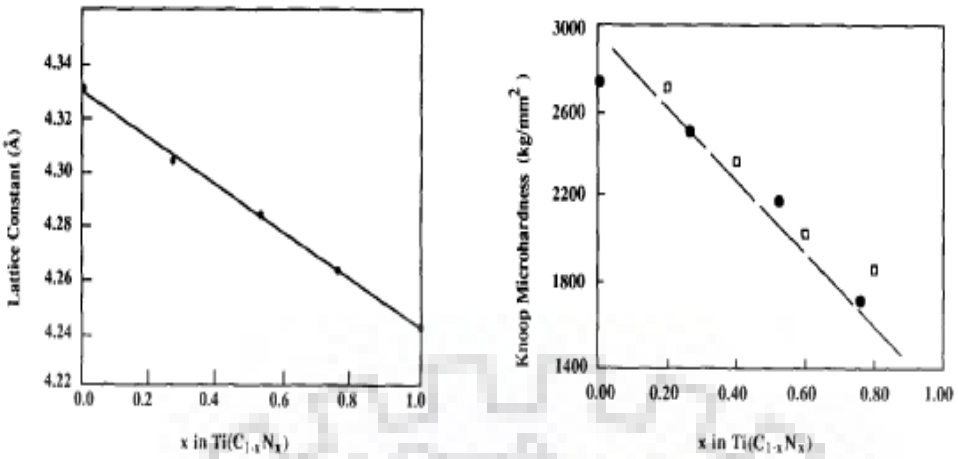

(a) (b)

Fig 2.2 Variation of lattice parameter and knoop hardness with $TiC_{1-x}N_x$ [2]

Table 2.1 shows that the properties of TiCN lies in between the properties of TiN and TiC it is a continuous solid solution of both TiC and TiN

Table 2.1: The major properties of TiC, TiN and TiCN [3,4]

Properties	TiN	TiC
Molecular weight	61.9	59.9
Crystal Structure Type	NaCl	NaCl
Unit Cell parameter(nm)	0.4240-0.4249	0.4318-0.4328
Melt point(K)	3223	3340-3530
Density (g/cm^3)	5.39-5.44	4.9-4.93
Thermal Conductivity($W.m^{-1}K^{-1}$)	29	17-24
Coefficient of thermal expansion(10^{-6} /K)	9.35	7.4-7.95
Micro-harness (HV, GPa)	20-20.5	30-32
Modulus of elasticity (GPa)	251	315-450

Ti(CN) has the beneficial benefits of both the compounds as it is a solid solution of both TiC and TiN (high thermal conductivity, high hardness, high melting point etc) [3,4]. But Ti(CN) has a very low toughness (3-4 MPa√m) making it very brittle.

2.1.2 Microstructure

Ti(CN) based cermets have a typical microstructure consisting of phases depicting the dissolution of solid phases, generally categorized into three phase namely hard phase, binder phase and surrounding phases. Ti(CN) based cermets have a core-rim type structure in which

the core is at times divided into two parts called outer and inner rims. The hard phase is commonly believed to be made up of undissolved Ti(CN)/TiC powders surrounded by rim phase which consists of a complicated phase (Ti,W,Mo,V,…..)(CN) having similar structure as that of core but different as it contains more heavy elements than that of core. Thus due to this the core appears to be dark while the rim phase having high concentration of heavier elements appear light when seen in a FE-SEM (BSE) image[8].

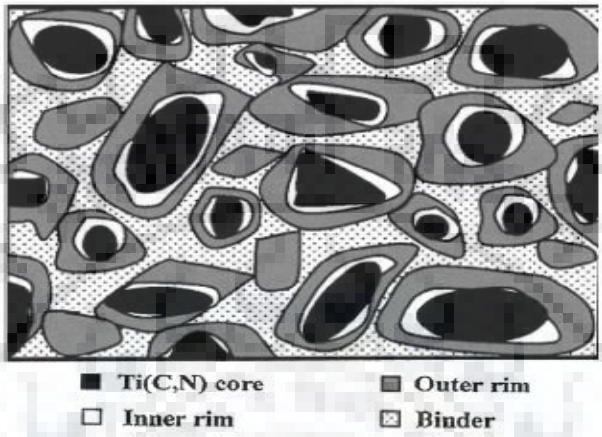

Fig2.3 Schematic representation of SEM image of typical Ti(CN) based cermets[9]

From Fig 2.3 it can be seen that inner rim appears lighter than to outer rim as it contains heavier elements. The rims are formed by different process, outer rim formed during solid state sintering and inner rim is formed during liquid phase sintering by dissolution re-precipitation of secondary carbides [10].

Formation of core-rim structures follows the Ostwald dissolution-precipitation mechanism [11]. Dissolution of smaller grains is much higher as compared to the large grains [12] as it is thermodynamically favourable. Thus at the time of sintering the smaller grains dissolves rapidly as compared to the larger ones. Simultaneously Ti(CN) grains continue to dissolve and precipitate in undissolved grains[13] resulting in the formation of complex carbides on the undissolved Ti(CN) particles. Also at elevated temperature N atoms are released resulting in the Ti(CN) dissociation replacing C atoms thus converting complex carbides into complex carbo-nitrides (Ti,W,Ta,…..)(C,N).

2.1.3 Grain Shape Accommodation

In liquid phase sintering the molten binder acts as the site for dissolution and precipitation which occurs during the sintering. The molten binder phase forms a canal like structure as it flows into every vacant position and thus it helps in the grain coarsening, which in turn helps in the formation of core and rim like structure in the microstructure. There are two phenomena which determines the shape of the core-rim structure i.e. solution re-precipitation control growth and reaction precipitation [36,37]. Solution re-precipitation control growth results in the formation of spheroidal grains while reaction precipitation results in polyhedral core-rim structure.

The volume fraction of liquid is the key factor to determine whether or not the grain shape accommodation will occur or not. It is normally favoured when the amount of liquid is insufficient to completely fill the voids, thus resulting in polyhedral grain shape. Due to large amount of liquid, capillary pressure is low, so driving force for contact flattening and shape accommodation is reduced thus maintaining the spheroidal grain shape [37].

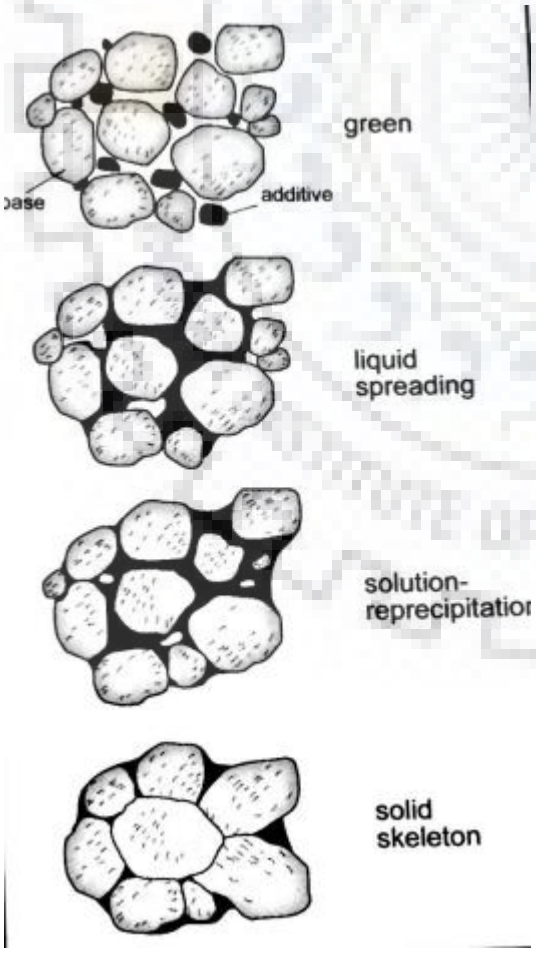

Fig 2.4 The conceptual stages of liquid phase sintering of a mixed powder for two or more powder composition [36]

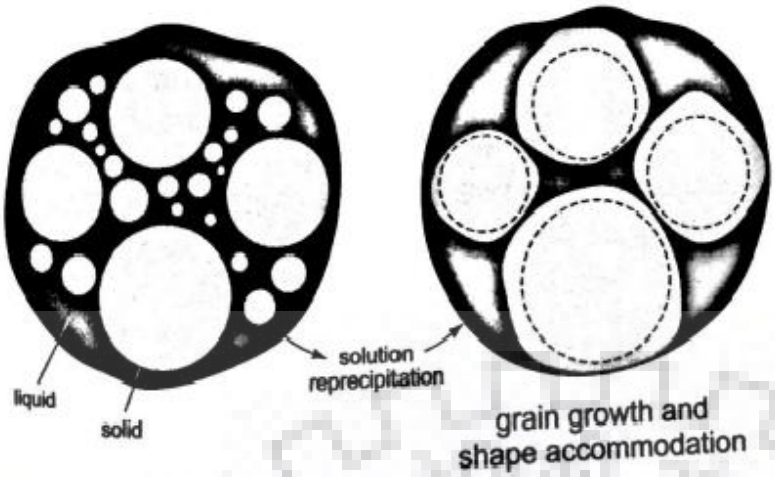

Fig 2.5 Solution re precipitation controlled grain growth reaction mechanism [36]

During liquid phase sintering the solid grains undergoes shape accommodation where the flat faces form on neighboring grains allow closer fitting together. Grain shape accommodation releases liquid to fill any remaining pores, thus leading to a formation of rounded grain particles.

2.2 Effect of various constituents on mechanical properties of Ti(CN) based cermets

2.2.1 Effect of carbon and nitrogen

Carbon increases the hardness of Ti(CN) cermets and when present in alloying elements, it has been confirmed [14] that it inhibits the dissolution of carbides in the binder phase and thus reduces the thickness of the rim. Thin rim phase results in improved transverse rupture strength[15,16] and also it leads to good densification due to enhanced wettability on the account of proper degassing of oxygen adsorbed on the powder particle surface.

Addition of TiN to TiC based cermets refines the core size and also reduces the thickness of the rim while excess TiN deteriorate the mechanical properties due to the decrease wettability of the hard phase, imperfect rim structure, growth of core size [17]. Ti(CN)-based cermets modified with TiN possess a higher thermal shock resistance than one without.

2.2.2 Effect of Binder

Addition of Co to Ti(CN) based cermets have resulted in improved toughness and resistance to oxidation as compared to Ni-based cermets because Co has high toughness as compared to Ni and improved wettability of the hard phase [14]. Addition of Co to Ni basic binder phase has resulted in increased machinability and also lowers the solubility of hard phase into binder [18]. Weight fraction of Ni/(Ni+Co) is kept in between 0.3-0.8.

One of the most significant binder used in various types of cermets. Ni is responsible for better toughness and its addition has resulted in increased density, high corrosion resistance, less environmental pollution, prevention of balls abrasion in ball milling. Ni addition also prevents the carbide particle agglomeration and is capable of forming a uniform structure with fine particles [18]. Excellent wear resistance is derived from hardness of the ceramic particles and binder toughness.

Zhou et al. [19] reported that the fracture toughness of Ti(CN) cermets reached its maximum value at 20% and 25% binder phase addition for grain size varying from 2-3 μm, respectively. Increased addition leads to decline in fracture toughness which is related to stress concentration in metal phase due to increase in metal layer thickness between the ceramic particles.

Mo has been reported [20] to improve the mechanical properties. Also it increases the wettability between the binder and the ceramic phase because a Mo-rich shell around ceramic particle is formed, as referred from reference [20] Ni has poor wettability. Mo-rich shell encompassed the whole ceramic particle and acted as a modificator because of the lack of ceramic particle agglomeration in the matrix leading to decrease in contact angle between the liquid matrix and the ceramic particle [21].

Grain growth can be limited during sintering because Mo decline solubility in the binder than carbides or carbonitrides phase, thus the solid precipitation mechanism was hindered by the lack of solution of ceramic particles in the binder [22]

2.2.3 Role of secondary carbides:

For good sinterability the prerequisite is good wettability but that does not necessarily results in good bonding. Contact angle between two phases is also a necessity. Thus for wetting to occur the contact angle should be between 0-90°. Various requirements for good wetting are:

i. Contact angle between carbide and liquid melt decreases with decrease in negative heat of formation [23]

ii. Preferential adsorption of atoms at interface and lowering interfacial energy or when diffusion gradient is established across solid-liquid interfaces thus reducing the contact angle

Mo_2C has the lowest negative heat of formation (-17.6 kJ/mol) and therefore it has lowest wetting angle thereby making it an indispensable component in commercially made cermets**.**

Previous studies has shown that WC reacts with Ti(CN) to form a complex phase (Ti,W,X…..)(CN) which surrounds the undissolved raw Ti(CN) particles. Thickness of binder phase decreases with increasing WC addition which indicates that wettability of binder phase with complex (Ti,W,X…)(CN) increases resulting in better continuity of the binder phase. From reference [24,25], it has been found that transverse rupture strength increases on WC addition and this is due to the fact of increased wettability between hard phase and binder resulting from increasing bonding strength at the interface perfectly explained by Griffith-Orowan equation

$$\sigma = (2EP/\pi L)^{1/2} \quad \text{……eq. 2.1}$$

where E is Young's modulus, P is plastic deformation due to crack strengthing and L is length of the crack

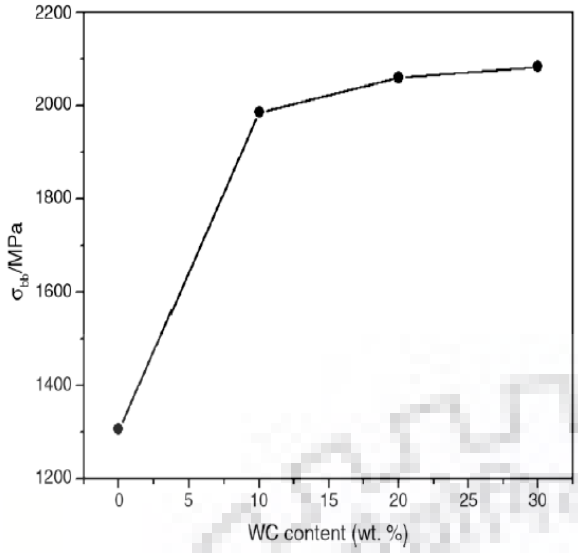

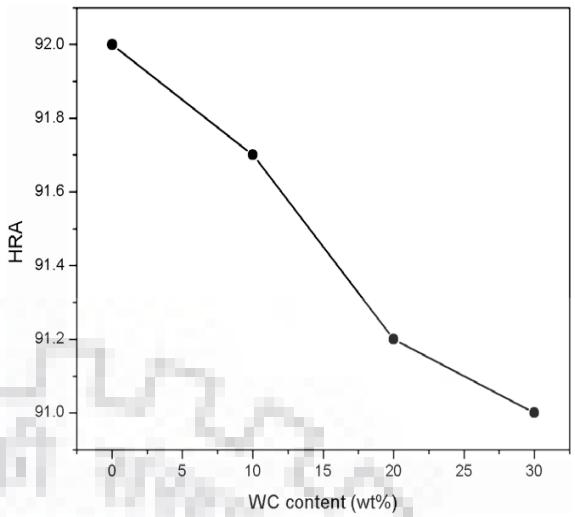

Fig 2.6 Effect of WC content in TRS [24] Fig 2.7 Effect of WC content on hardness[24]

Ambiguity has been found to WC addition when it comes to hardness, as hardness decreases with increasing WC content as shown in Fig 2.7. Wang et al. found that hard phase grain size does not change because of Mo_2O presence in a Ti(CN)-WC-Mo_2O-(Co,Ni) system [25]. On the other hand Ti(CN) amount decreases on WC addition as more (Ti,W,Mo)(CN) is formed which reduces the hardness as compared to Ti(CN).

It has been shown in studies by Xiong J et al [24] has reported that particle size decreases as WC content increases. But after an optimum amount of 15wt%, WC starts to precipitate out resulting in decrease in hardness. Optimum WC addition content is reported to be 15 wt%.

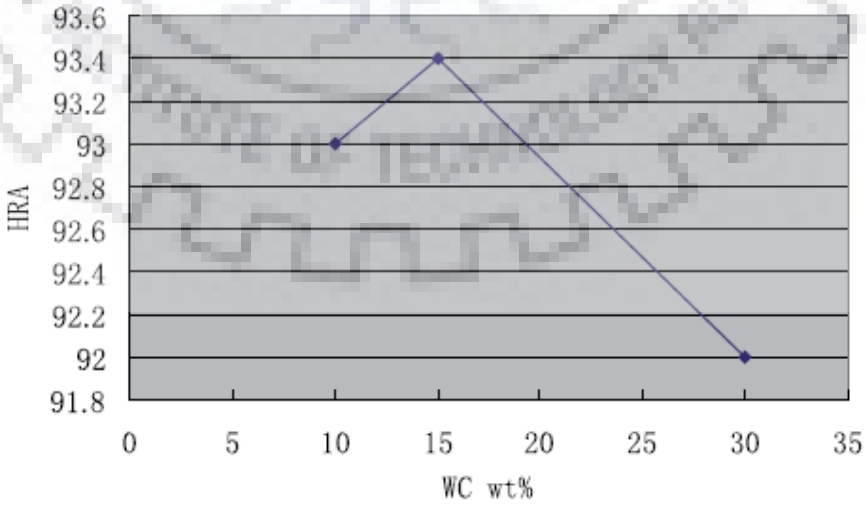

Fig.2.8 Effect of WC wt% on Hardness with WC content [24].

Mo_2C addition increases the wettability between hard phase and binder phase by forming a solid –solution of (Ti,Mo,X….)(CN) which is easily wetted by Ni-Co binder phase [24,26]. Sinterability is also enhanced on the account of increased wetting and thereby leading to greater mechanical properties. The rim of (Ti,Mo,X….)(CN) formed around hard Ti(CN) phase prevents grain growth by dissolution and precipitation thus leading to refinement of grain structure which leads to high transverse rupture strength as per Hall-Petch formula [26].

Addition of Mo_2C above the optimum limit leads to increased thickness of rim and degradation in mechanical properties [26]. Optimum content for Mo_2C addition is 10 wt%.

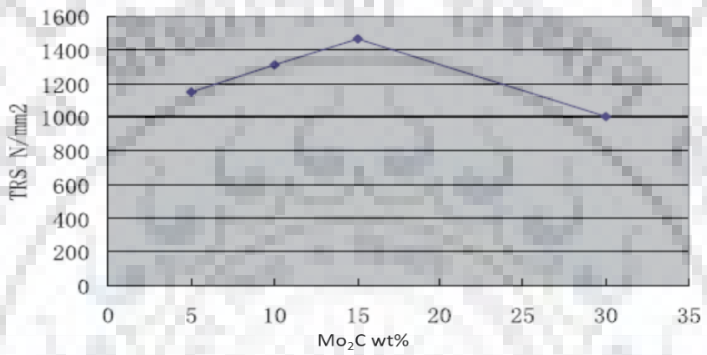

Fig 2.9 Variation curve of TRS with Mo_2C content.

From studies [26,27] TaC has been found to improve high temperature plastic deformation resistance of cutting tools and red hardness. Both bending strength and hardness decreases on TaC addition but microhardness been found to improve on TaC addition.

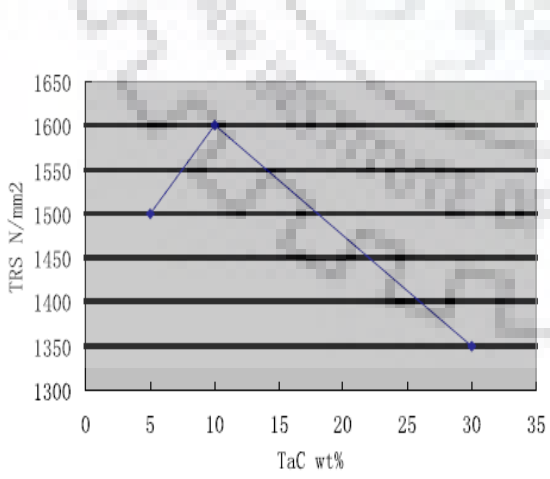

Fig 2.10 Variation of TRS on TaC content.

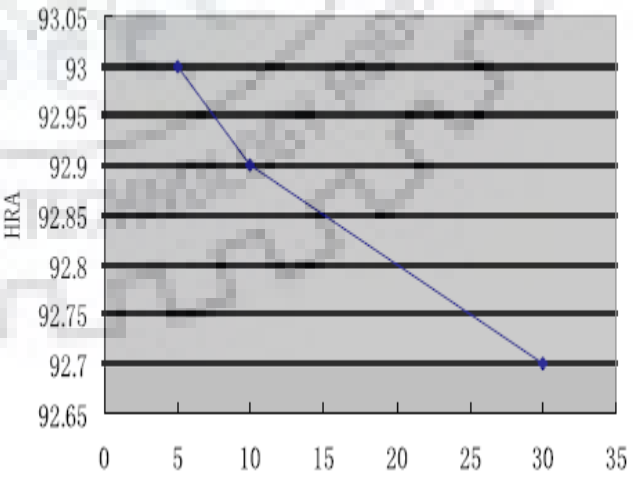

Fig 2.11 Variation of hardness with TaC content

TaC decreases the density of cermets on account of its poor wettability with hard phase and binder phase which can be explained from its enthalpy of formation (-161.1KJ/mol) which is

much higher than that of Mo_2C (-16KJ/mol) and WC (-35KJ/mol). Optimum amount of TaC i.e. 7 wt% has been reported.

NbC is a good substitute to costly TaC as it also improves the high temperature deformation resistance [28]. In presence of Mo_2C, NbC does not affect the rim thickness [29] but it has a strong effect on microstructure. Qi et al. found that at low concentration, NbC forms (Ti,Nb)(CN) rim phase around Ti(CN) particles. If added above optimum limit it starts precipitating around NbC grains because of its low solubility in hard phase and higher surface energy in liquid melt as compared to Ti(CN) grains.

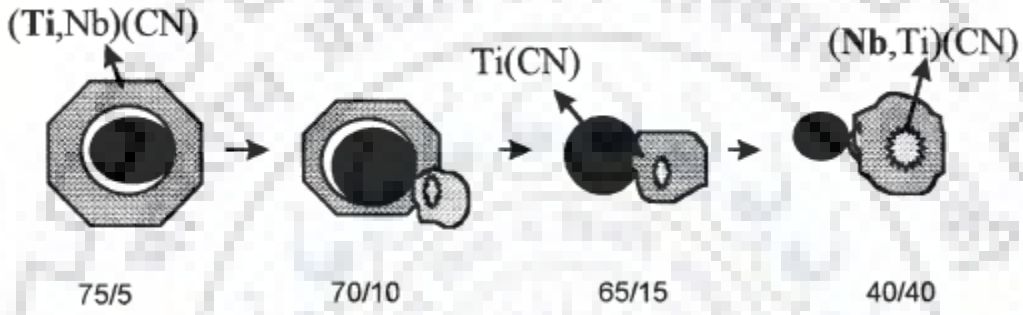

Fig 2.12 Schematic shows microstructure evolution with NbC content in Ti(C0.7N0.3)-xNbC-20 wt%Ni system [28].

The white phases shown in Fig 2.12 are nothing but undissolved NbC grains which are surrounded by grey rim phase. Jun et al. found that NbC can be used to improve sinterability for two reasons:

1. It helps to bring down sintering temperature
2. During liquid phase sintering it gets dissolved in liquid melt and therefore increases the amount of liquid melt, facilitating in easy densification.

Optimum limit of 10 wt% has been reported but above that limit porosity starts increasing and density goes down [28,29].

From reference [30] Cr_3C_2 acted as the effective grain growth inhibitor. It has been shown that mechanical properties are improved remarkably. It has also resulted in increase in both hardness and transverse rupture strength upon Cr_3C_2 addition. Hardness of the cermets increases with grain size decreasing. Small grain size increases the surface area of interfaces and enhance formation of galvanic couples on the material surface. Both of the factors leads to impairment in corrosion behavior [30].

2.3 Sintering Process

In order to obtain the best mechanical properties one has to sinter the components to a required temperature. But sintering is not only limited to one technique, it has many parts each having their own unique features. As referred [31,32] it has been proven that wear resistance of cermets increases with grain refinement and bonding strength between phases present. Conventional sintering methods which requires a high temperature holdings for a long period are tedious and are unable to accomplish our requirement leading us to choose better sintering methods.

The various important sintering technique are vacuum sintering (NS), hot isostatic pressing (HIP), microwave vacuum sintering (MVS), Spark Plasma Sintering (SPS) etc.

Table list the properties of various sintering methods.

Table2.2 Properties of cermets obtained via different routes [14].

Sintering Process	Hardness	Fracture toughness ($MPam^{1/2}$)	Bending Strength (MPa)	Grain Size (μm)
NS	11.2-12.3 GPa (HV)	12.6-13.2	-	0.03-0.1
NS	14.7 GPa (HV)	10.1	2210	0.5-1
NS	14-15 GPa (HV)	8-10	-	<0.3
HIP	93 HRA	-	1740	-
HIP	93.5 HRA	-	1740	-
HIP	92.6 HRA	-	1500	-
SPS	89.9 HRA	-	840-920	<0.3
SPS	91 HRA	-	295	<0.42
SPS	90.2 HRA	-	-	0.2
MVS	90.6 HRA	-	1547	0.5-1
MVS	91.6 HRA	-	-	<1

The major concern for sintering ultra-fine cermets is of coarsening as the conventional sintering technique subject sample to high temperature for an extended holding time resulting in unexpected grain growth. The driving force for sintering is reduction of surface energy, either by reducing the total surface or by replacing solid-vapor interface with solid-solid interface, the latter leads to densification. But the major issue was that these phenomena competes with one other [33].

Two major points have come to light from various sintering mechanism proposed:

i. Mechanism responsible for coarsening is surface-diffusion which is prevalent at lower temperatures.
ii. Extended holding times at elevated temperatures results in unwanted grain growth.

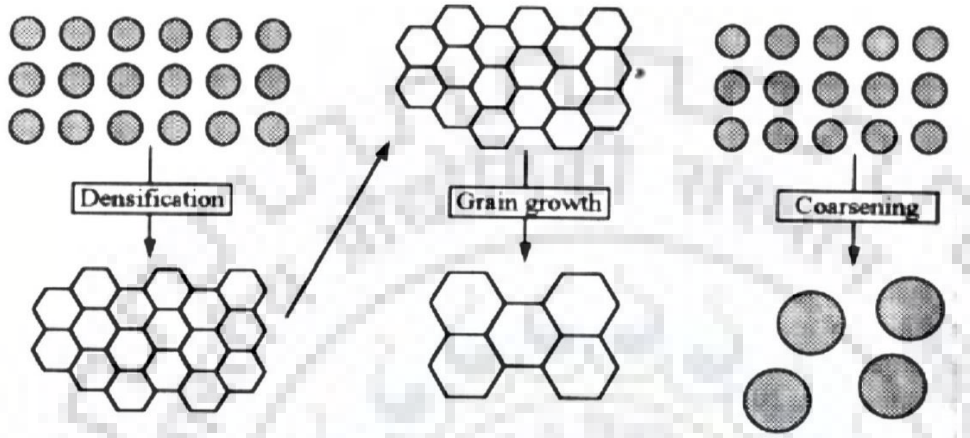

(A) (B)

Fig 2.13. (A) Schematic showing a typical densification phenomenon. (B) Schematic showing coarsening phenomenon [33]

This two problems was solved when we use SPS where one can achieve high heating rates and at same time can lower the holding time at elevated temperature.

Hot isostatic pressing sintering (HIP) can also solve this problem, as it has an inherent advantage over conventional process as it uses both pressure and temperature to sinter at the same time. Pressure helps in bringing the particles closer which in turn helps in augmenting the mass transfer rate. Its application contributes for the increased densification kinetics via

i. Reduced stress due to presence of larger interagglomerated pores
ii. Breakage of agglomerates
iii. Pore shrinkage via plastic deformation of grains

Still such process are time consuming and temperature required is high. Another concern is that with increase in pressure there is decrease in particle size. For instance, pressure

requirement for ultrafine powder rises to 500MPa as compared to only 5MPa in case of micro-sized powder compact.

$(\sigma = -2\gamma/r)$…… Eqn. (i)

σ Sintering stress

γ Surface tension

r Pore radius

It is clearly seen that as particle size goes down the requirement of sintering stress increases and in case of ultrafine cermets such stresses become so high, it becomes impractical to achieve.

Advantage of SPS over other sintering mechanism was that it was able to densify the sample at low temperature when compared to other sintering methods. Also it can give us high heating rate which allows us to control the grain growth and by which one can control the grain refinement to a certain degree.

SPS involve three major qualities which enables it to lower the severity of sintering conditions:

i. Like HIP, it is a pressure assisted sintering
ii. Involves physical activation of the particles
iii. Mechanism is such that it provides local heating effect at surface of powder particles which helps in restricting grain growth.

Due to spark discharge between the particles, ionizations in the gas column occurs between the powder particles leading to spark plasma, which in turns results in high temperature generation at the particle surface. This leads to high pressure between the powder particles that leads to spark impact and sputtering of molten particles which in turn reveals the virgin surfaces with high surface energy leading to necking between powder particles. In SPS due to joule heating between powder particles followed by initial plasma discharge [34], leads to sintering mechanism.

Various advantage of SPS are:

i. Only particle surface is heated so in absence of excess heat grain growth is prevented.
ii. Heat is supplied at a place where it is needed (lower power consumption).

iii. Localized pulse causes enhanced diffusion, thus preventing rapid sintering, thus preventing grain growth.

iv. SPS ensures a very fast heating rate and short holding times at low sintering temperatures, which all prevent grain growth.

Its major disadvantage is that it limits mass production and limited shapes.

2.4 Wear of TiCN based cermet

The major purpose to design and develop TiCN based cermets is to achieve advance tool materials that will be able to withstand the severe conditions of high speed machining. Thus it becomes necessary to study the wear characteristics of cermets. Generally during machining, a numerous wear phenomena takes place, namely fretting wear, sliding wear, erosive wear, crater wear, creep etc. The present work focuses on the sliding wear of TiCN based cermets.

According to Gahr, 1987 the wear and induced friction for any sliding couple is contributed by many properties such as, surface finish, load, speed, shape and dimensions of the coupled solids, adsorption of atoms, material composition, lubrication, humidity and metallurgical parameters. Sliding wear can be performed at laboratory scale by using various test configuration, pin-on-disc, ball-on-disc etc. For TiCN based cermets sliding wear is influenced by their microstructure and mechanical properties. Literature survey shows that the test is usually carried out at room temperature (25±5℃) with a relative humidity of 30-40%. The complex tribological behavior of Ti(CN) based cermets in sliding wear is widely characterized by tribochemical wear, abrasion, adhesion, oxidation, plastic deformation and/or fracture.

Peng et al. [14,39] observed tribological changes with the addition of secondary carbides. Increasing the WC content has shown improvement in wear resistance of the cermets [39]. According to [39] load dependent sliding wear and friction properties of TiCN-20Ni-xWC, where was varied from 5wt% to 25wt%, at lower loads (<5N) abrasion and mild tribo-oxidation was the dominant wear mechanism while at higher load (>20N) dense tribo-oxide layer formation was the dominant factor when sliding as done against steel.

Table 2.3 Summary of tribological characteristics of Ti(CN) based cermets during sliding against different counter-bodies in dry condition [52]

Cermet composition	(Ti(CN)-20Ni)-WC/NbC/TaC/HfC	TiC-NiMo	(WC-Co)-TiC,TaC/NbC	Ti(CN)-Ni-WC	Ti(CN)-Ni-Mo	Ti(CN)-Al2O3-Ni-Mo
Counter body	Steel	Steel	Steel	Steel	Si_3N_4	Si_3N_4
Dry (in air) sliding wear test conditions	300 rpm; 5, 20 or 50N	2.2m/sec; 40N	1500-3000rpm; 40N-350N	0.1m/sec at 5, 20 or 50N	0.5m/sec; 5N	0.5m/sec; 5N
COF	0.4-0.7	0.2-0.3	0.2-0.7	0.23-0.73	0.8	1.0
Wear rate (mm^3/Nm)	$10^{-6} – 10^{-7}$	$3.8x10^{-7}$ -$13x10^{-7}$	-	$2.7x10^{-7} – 3.4x10^{-7}$	10^{-7}	10^{-7}
Dominant Wear mechanism	Tribolayer removal	Tribo-layer removal	Tribofilms removal	Tribolayer removal and deamination	Mirco fracture	Tribo-layer removal

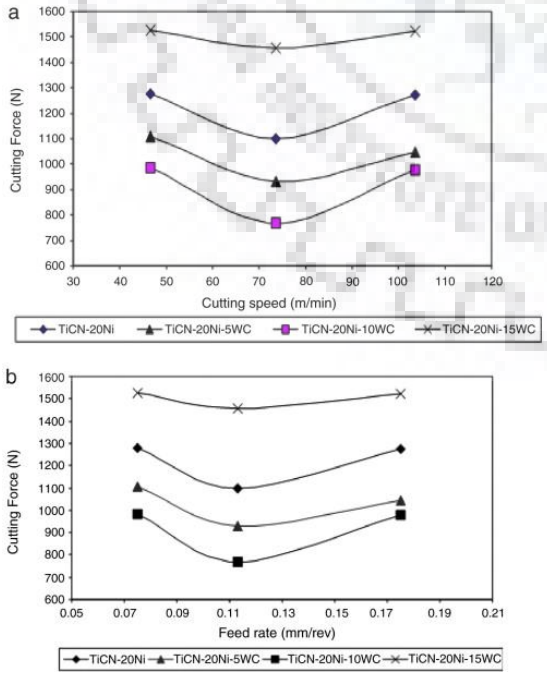

Fig 2.14 Variation of cutting force with respect to (a) cutting speed and (b) feed rate of TiCN-based cermets with different addition amounts of WC[39].

In this chapter, all the experimental procedure involved in preparation, characterization and wear testing of TiCN based cermet has been explained. Sample is prepared by tumbler milling and the mixed powder is then sieved and then various steps are taken along to get the final result. Steps involved are spark plasma sintering, density calculation method, XRD analysis and wear characterization.

3.1 Material preparation

Powders received are Ti(C_xN_{1-x}) (where x=0.5, purity 99.8%, particle size-40nm), WC (purity 99%, particle size<800nm), Ni (purity 99.5%, particle size <1µm), Co (purity 99.5%, particle size<1µm), TaC (purity 99%, particle size<2µm). The XRD pattern of as received powders are shown in fig. 3.1.

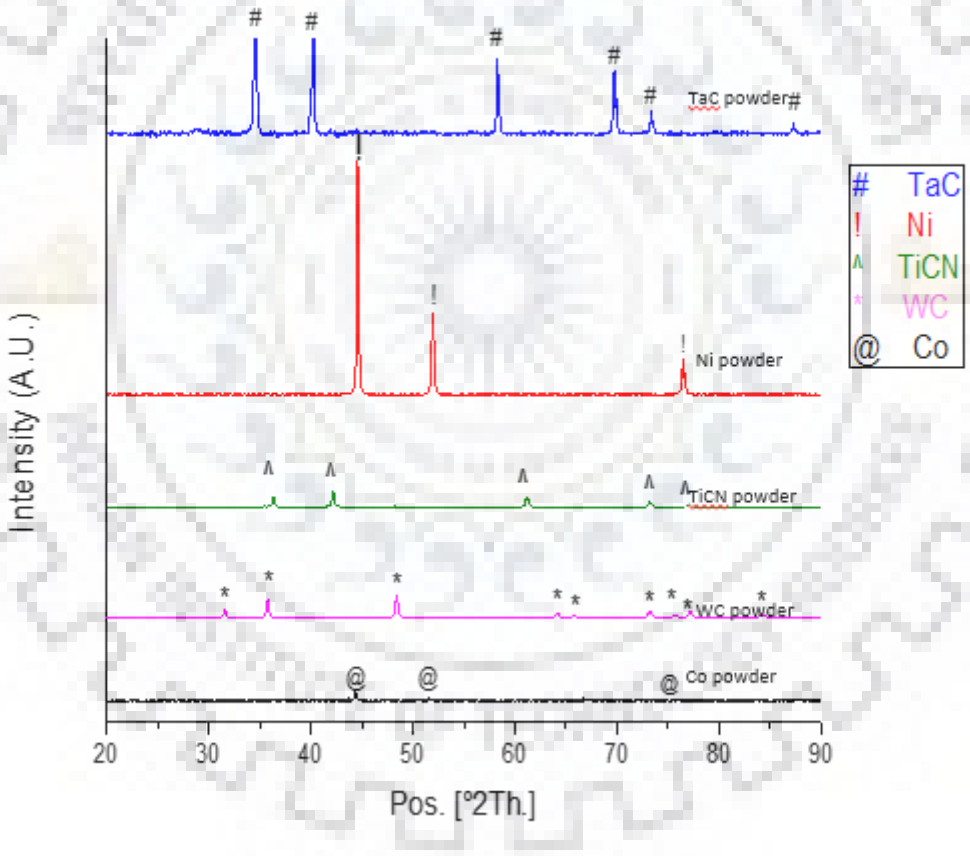

Fig 3.1 XRD graph for the received powders

Sample for the test is made in such a manner that apart from Ti(CN) all other components are taken as 10 wt% in the overall mixture. The powder was mixed with the help of tumbler miller and the process was carried out for 24 hrs, in order for the powder to mix completely.

WC-Co balls were used to mill the powder and the powder was kept in a plastic bottle after dipping the powder and ball in toluene. The ratio of powder to ball weight was kept at 1:10. The final composition of the sample is Ti(CN)-10wt%WC-10wt%TaC-10wt%Ni-10wt%Co.

3.2 Ultrasonication

The milled powder was ultrasonicated before it went for sintering process. This was done to avoid some or any agglomeration that might come during the milling as it may impact the microstructure of the sintered samples. The powder was dipped in acetone and duration for the process was about one hour.

3.3 Spark plasma sintering

Currently the sintering technique used for work is spark plasma sintering (SPS-625,Fuji Electronics Ltd., Japan). Here the parameters like temperature, pressure and heating rate can be controlled which in turn can help in controlling the grain growth needed for making the material dense.

Fig 3.2 Photograph of spark plasma sintering machine.

In order to get a dense material, the temperature was varied from 1200℃-1500℃ while keeping the holding time constant at 3 min. The pressure was also kept constant at 40 MPa but the atmosphere for the initial three samples it was Argon atmosphere while for the remaining three it was kept in vacuum. Also the heating rate was varied, 100℃/min for first three trials and 600℃/min for last three. Sintered samples were polished on a belt polisher to remove the graphite layered adhered to it during sintering, and the samples

were polished on an auto polisher using suspension of diamond particles of 45µm, 15 µm, 6 µm, 1µm size.

Table 3.1 Various SPS trails for the composition Ti(CN)-10wt%WC-10wt%TaC-10wt%Ni-10wt%Co

Designation	Temperature(℃)	Holding time (min)	Heating Rate (℃/ **min**)	Pressure applied
S1	1200	3	100	40MPa (Ar)
S2	1300	3	100	40MPa (Ar)
S3	1350	3	100	40MPa (Ar)
S4	1500	3	600	40MPa (Vac)
S5	1500	3	600	40MPa (Vac)
S6	1500	3	600	40MPa (Vac)

3.4 Density calculation

The density of the sintered sample was determined using Archimedes principle. The sample was weighed initially in air and then it was immersed in water. The weight was measured in both conditions and the following formula was used to determine the density of the sintered sample.

$$\boldsymbol{D = weight\ in\ air/(weight\ in\ air - weight\ in\ water)} \quad \text{.....eq. 3.1}$$

Theoretical density of powder mixture was measured using the rule of mixture as

$$1/\rho = w_1/d_1 + w_2/d_2 + w_3/d_3 \quad \text{.....eq. 3.2}$$

where ρ is the theoretical density of composite.

w_1, weight fraction of first component.

d_1, density of first component.

The C/N ratio in the Ti(CN) powder is 7/3 which is the best C/N ratio. The major issues which arises will come if C/N ratio is different. Studies had shown that the optimum limit of WC and TaC addition is 15wt% and 7wt% respectively.

3.5 Microstructural analysis

There is development of core rim binder phase morphology in the material which is visible in SEM micrographs of the sintered cermets with black, gray and white contrast. The microstructural parameters were evaluated by linear intercept method for each cermet microstructure. ImageJ Analyser was used to estimate the average particle size of core and rim in microstructure of the cermets along with linear intercept method.

3.6 Mechanical properties

3.6.1 Micro hardness analysis

The hardness of the material was calculated using a Vickers Hardness Indentation machine. The applied load was of 3 kgf for calculating the hardness of the material and the diagonals were measured. The hardness was calculated using the formula

$$\boldsymbol{Hv = (1.8544 * P)/d^2} \quad \text{.....eq. 3.3}$$

Where, P is load applied

D is the mean of diagonals from indentation

3.6.2 Fracture toughness

Fracture toughness is measured using the crack length generated during the indentation made by the Vickers Microhardness Tester. The load applied is of 10 kgf for a dwell time of 15 sec The formula used for fracture toughness measurement is as follows:

$$\boldsymbol{K1c = \beta\sqrt{(H * \frac{P}{4a})}} \quad \text{.....eq. 3.4}$$

where

K_{1C} stands for fracture toughness

H is hardness.

P is applied load.

$\boldsymbol{\beta}$ is the non-dimensional constant dependent on indenter geometry

a is radial median crack (as shown Fig)

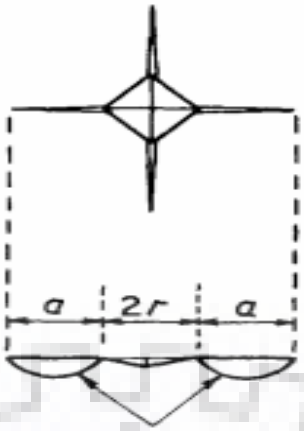

Fig 3.3 Formation of crack around the indentation mark showing radial median crack length "a".

3.7 Sliding wear

The sliding wear was done for samples whose sintering parameters were different to determine the coefficient of friction on different same load. The load was maintained at 10N and the speed of the disc was kept at 500 rpm. Three readings were taken for each sample and the time duration was kept for 45 min. The ball used for sliding wear was of WC-Co balls and the wear diameter was kept at 3mm.

The machine used was a ball on disc sliding contact wear and friction testing (TSE- 201E). Three readings for each sample were taken and then the debris were collected and checked in SEM to determine its constituents. A surface profilomer was used to determine the depth and width of the wear tracks. The wear volume was determined. SEM-EDS analysis of the wear tracks revealed dominant mechanisms of material removal.

This chapter deals with the results and its consequent discussion which arose from experimentation. It has been divided in seven sections, where the first section deals with the XRD analysis of the un-sintered and then the sintered sample. The third section deals with the SEM analysis of those samples and fourth section deals with the mechanical properties. The last three section deals with fracture morphology, the sliding wear test which was done to determine its wear characteristics and the SEM analysis of the wear tracks.

4.1 Mixing of powders

The mixture of the composition is done with weight percentage to make the composite i.e. Ti(CN)-10wt%WC-10wt%TaC-10wt%Co-10wt%Ni. The average size of the particles after mixing it in tumbler for 24 hours is 0.58μm. This was confirmed by using Laser Particle Size analyzer.

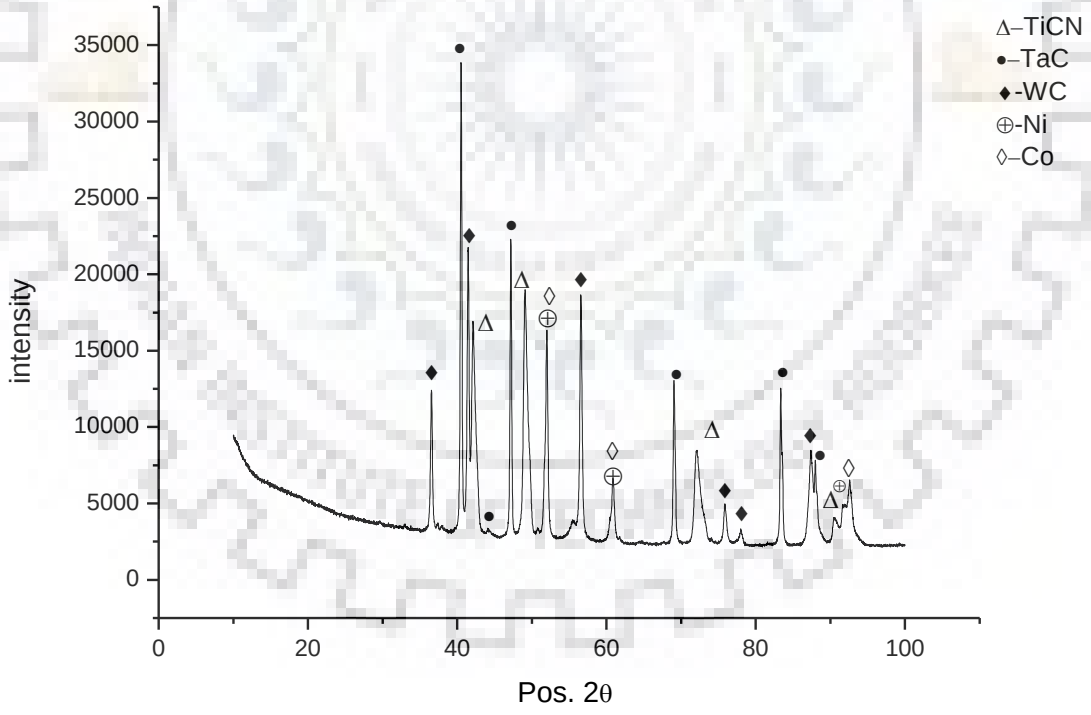

Fig 4.1 The XRD analysis of mixed powder

The XRD analysis of the mixed powder before sintering was done and the results are shown in Fig 4.1, it indicates that there is no presence of oxides nor any other impurities.

Ultrasonication was done to remove the agglomeration that was coming even after milling of powders. This method was chosen for the sole reason that one of the constituents of the powder is of nano-sized that is TiCN powder whose size is around 40nm as compared to the other constituents whose size are in the micro range.

4.2 Spark plasma sintering

The unique characteristic of SPS process is "Physical Activation of Surface" enables to speed up the reaction kinetics, which has been confirmed in and the present work has also proved this point. As compared to normal furnace which takes several hours for completion, SPS takes only few minutes for completion. The sample used was Ti(CN)-10wt%WC-10wt%TaC-10wt%Ni-10wt%Co.

4.2.1 Optimization cycles

The results of six SPS trials along with their XRD-analysis are discussed for the sintered samples.

Trail 1: The temperature of the sintering condition was kept at 1200℃ for 3 min.

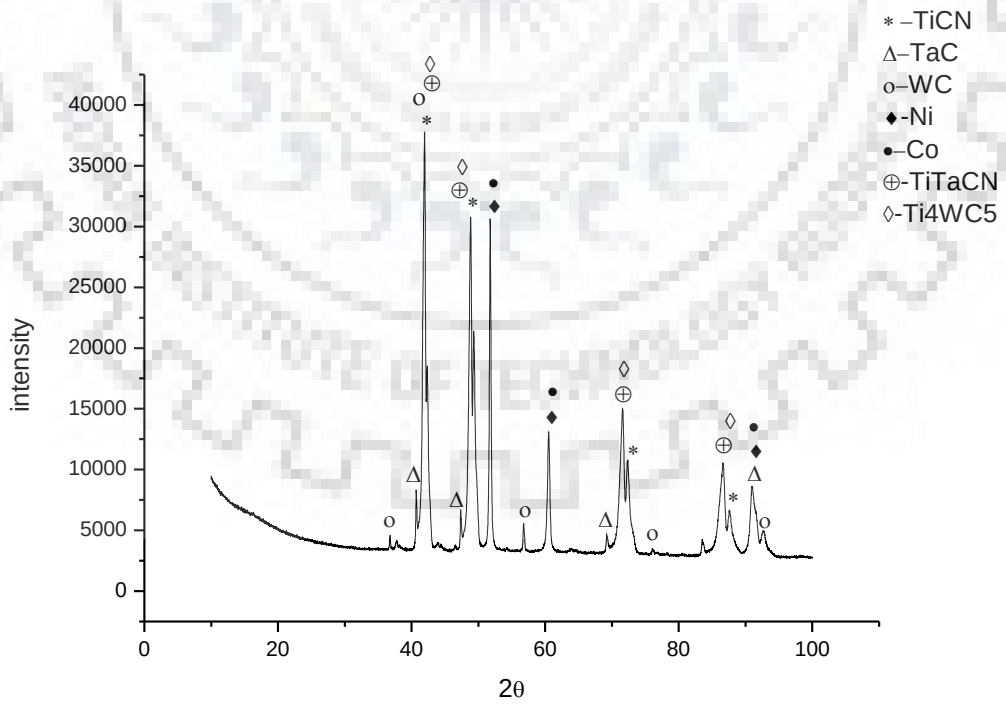

Fig 4.2 XRD of sample sintered at 1200℃

Trail 2: Final temperature was kept at 1300℃ for 3 min at 40MPa of argon atmosphere

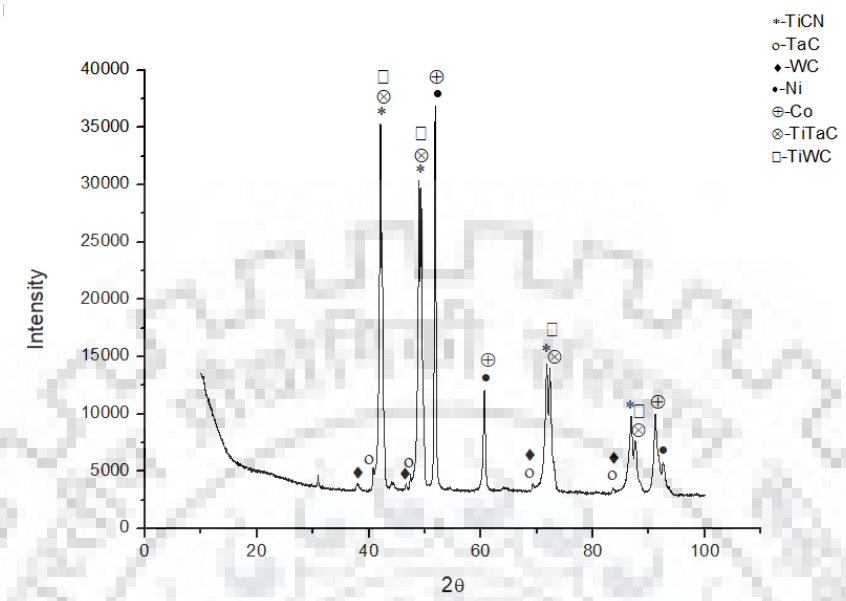

Fig 4.3 XRD analysis of sintered sample at 1300℃

Trial 3: Final temperature was kept at 1350℃ for 3 min. It shows the presence of Titanium oxide along with Titanium Tungsten Carbide and Titanium tantalum carbonitride.

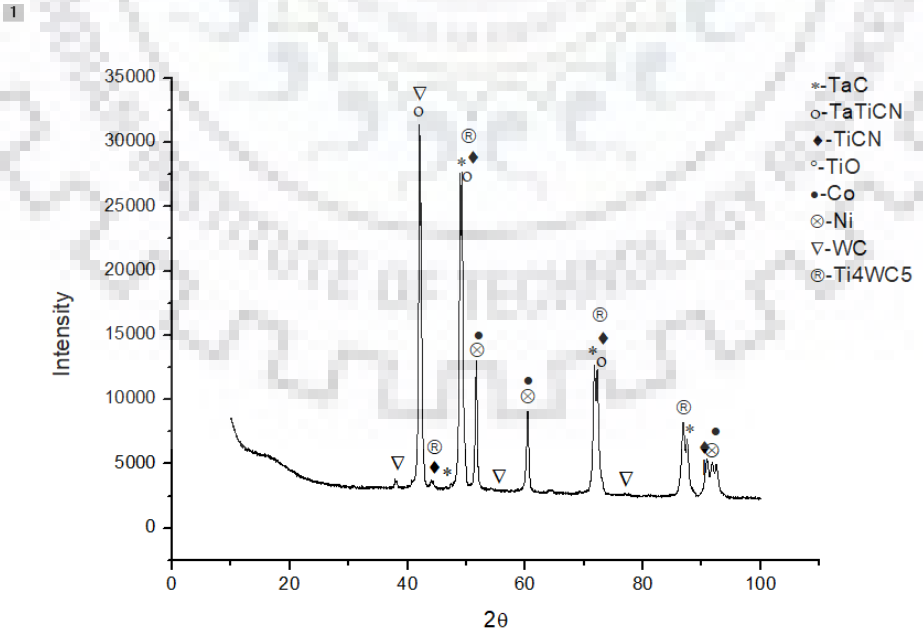

Fig 4.4 XRD analysis of sample sintered at 1350℃

Trail 4: Final temperature was kept at 1500℃ for 3 min in vacuum atmosphere where was the pressure maintained at 40MPa in vacuum atmosphere. It also shows the presence of Titanium Tantalum Carbonitride.

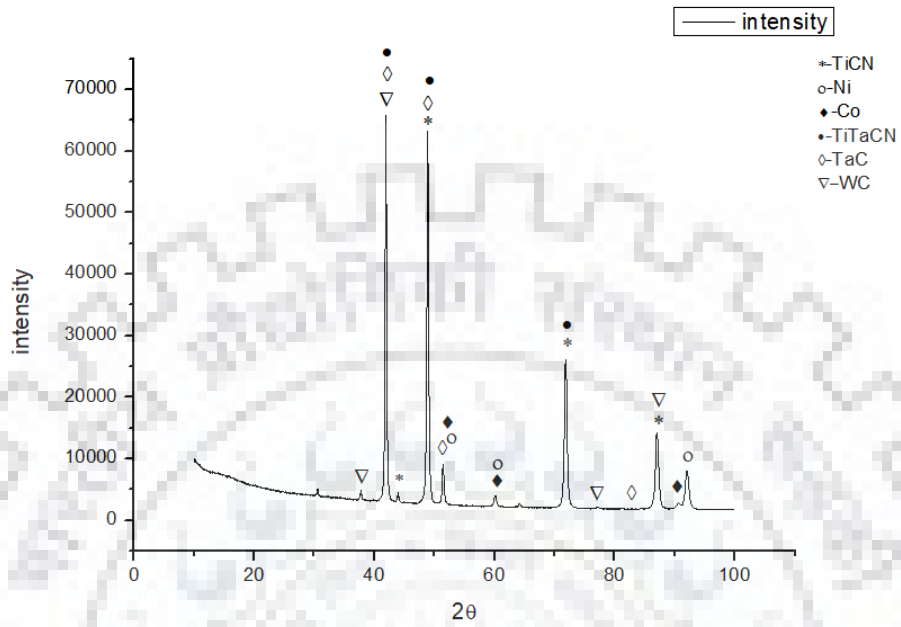

Fig 4.5 XRD analysis of sample sintered at 1500℃

Trial 5: Final temperature was kept at 1500℃ for 3 mins. Here there is no oxide present only composite mixture of Ti, Ta, W are present.

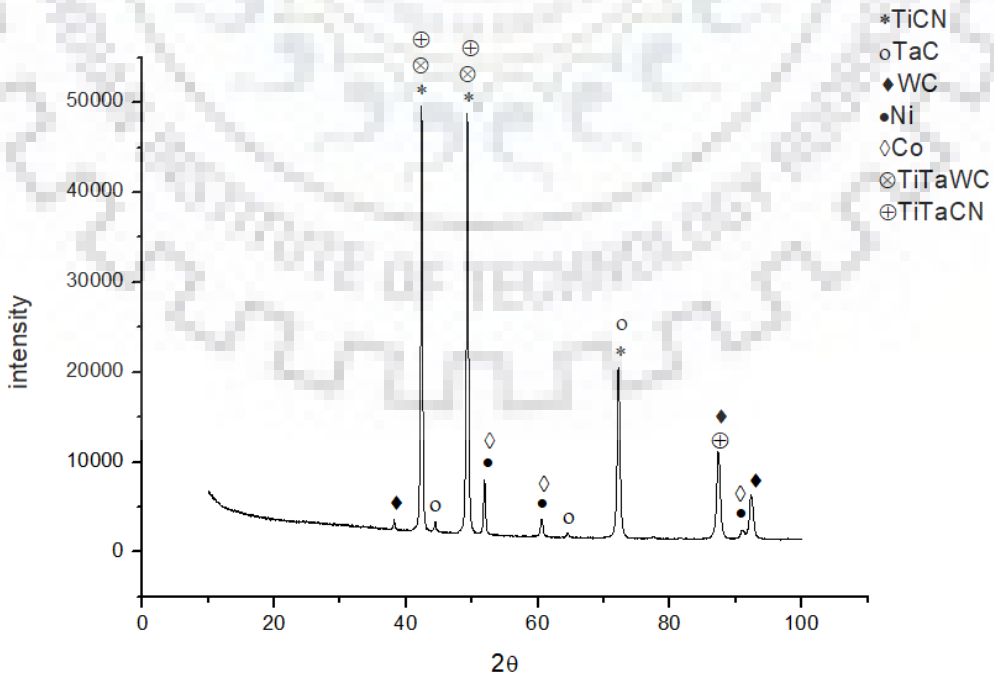

Fig 4.6 XRD analysis of sintered sample at 1500℃

Trail 6: The sample broke down during the removal from die so it was used to study the fracture morphology which is discussed later in this section.

Overall the optimization helped in determining the optimal temperature which gives us the densest material along with fewer oxides in the mixture which has been detailed in the Table 4.1 below

Table 4.1 Details related to optimization trials

	Trail 1	Trial 2	Trail 3	Trail 4	Trail 5	Trail 6
Designation	S1	S2	S3	S4	S5	S6
Temp (℃)	1200	1300	1350	1500	1500	1500
Heating rate (℃/**min**)	100	100	100	600	600	600
Time (min)	3	3	3	3	3	3
Amount (gm)	2.5	2.5	2.5	2.5	2.5	2.5
Atmosphere	Ar	Ar	Ar	Vac	Vac	Vac
Presence of oxides	No oxides	No oxides	TiO	No oxides	no oxides	Nil

4.3 Density calculation

Density was measured by Archimedes principle and the values are given in the table below.

Table 4.2 Relative density values of sintered samples

Sample designation	Relative density (%)
S1	84
S2	94
S3	94.6
S4	95.8
S5	94.8
S6	-

4.4 SEM analysis

The XRD analysis reveals the formation of (Ti,Ta,W)CN solid solution around the undissolved TiCN grains. This phenomena is confirmed with SEM-EDS analysis of different phases present in the microstructure of the sintered samples. Also point analysis, line mapping and elemental mapping was done to determine the phases which were present. At the time of sintering liquid phase is formed due to melting of Ni and Co. The carbides present get dissolved into the melt resulting in the start of dissolution and precipitation process known as Ostwald-ripening. The resulting microstructure is of core-rim structure where the dissolved carbides start to precipitate around the undissolved carbides which forms the core and the solid-solution on the periphery around the core is called rim mostly consisting of precipitated carbides. The rim phase helps in increasing the wettability of carbide powders by liquid melt.

The microstructure that is revealed after SEM is different as compared to the most shown in published research. This is due to solid-solution re-precipitation control growth reaction. As discussed in the literature, this occurs due to grain shape accommodation which is the direct result of the presence of high liquid content (binder phase) during the liquid phase sintering. Due to excess volume of molten binder phase during the liquid phase sintering, the grain takes a spheroidal shape in the microstructure instead of polyhedral shape.

The thickness of the rim is more which indicates that the binder is completely used during the sintering process. According to previous studies the thickness of rim is very minimal but here it is more which indicates that the binder phase is completely used to dissolve the carbides and for precipitation.

4.4.1 Mixed powder

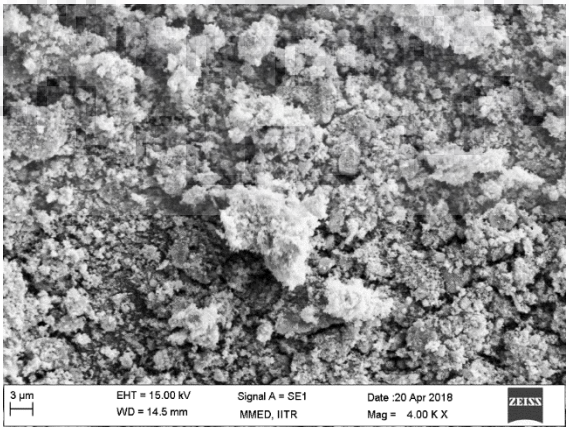

Fig 4.7 SEM image for the mixed powder

The average particle size from the above image can be seen to be around 0.6 nm which is in conjugation with the Laser particle size analysis. Also the maximum particle size shown in the image is of about 3micrometere which is the largest particle due to agglomeration.

4.4.2 Sample at 1200℃ (S1)

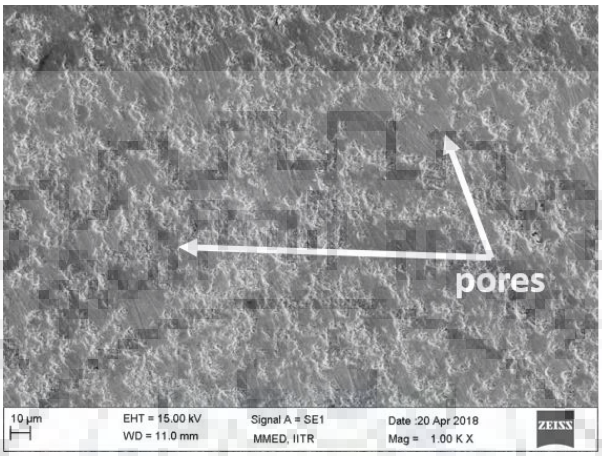

Fig 4.8 Material sintered at 1200℃ is highly porous

The SEM and EDS analysis reveals the presence of core-rim structure. Point analysis, line analysis and elemental mapping were done to find the presence of elements in the sintered material.

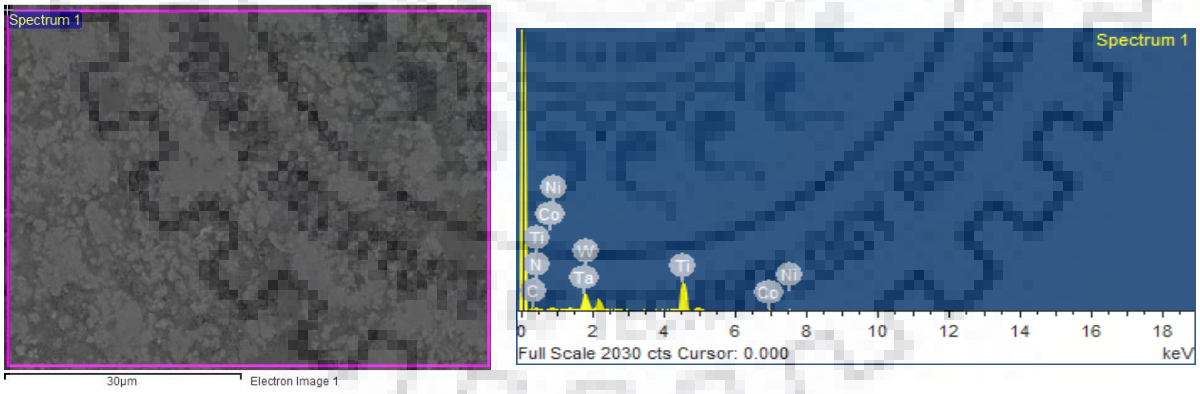

Fig 4.9 BSE and FE-SEM EDS analysis of sample sintered at 1200℃

Element	Weight%	Atomic%
C K	4.43	15.86
N K	9.14	28.05
Ti K	43.56	39.08
Co K	9.05	6.60
Ni K	4.89	3.58
Ta M	16.90	4.01
W M	12.02	2.81
Totals	100.00	

Table 4.3 Show the weight distribution of various elements present of S1

The area analysis reveals the presence of various phases in the sample. Line mapping and elemental mapping shows the location of various elements and phases which it forms after sintering.

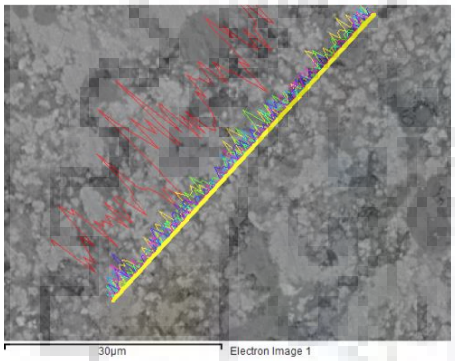

(a)

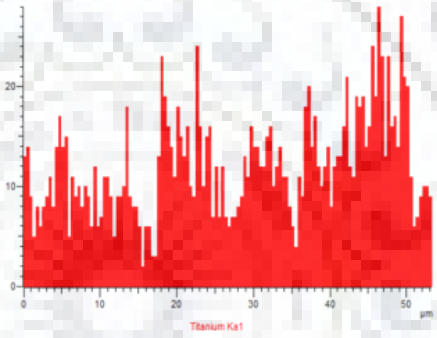

(b)Ti

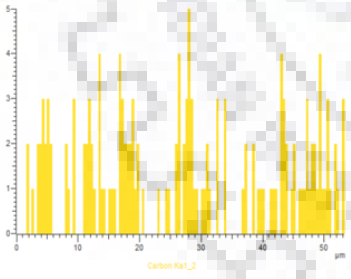

(c)C

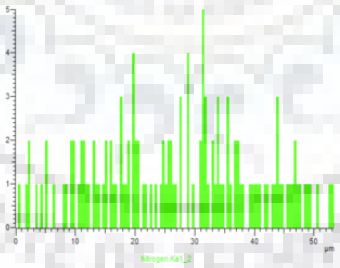

(d)N

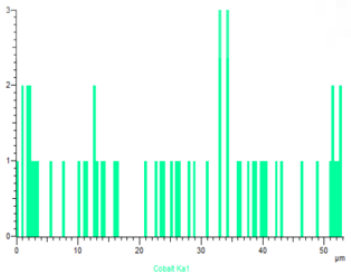

(e)Co

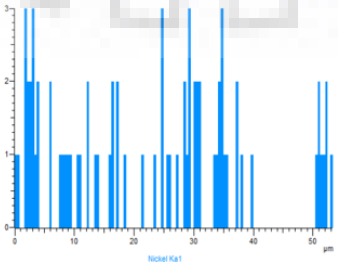

(f)Ni

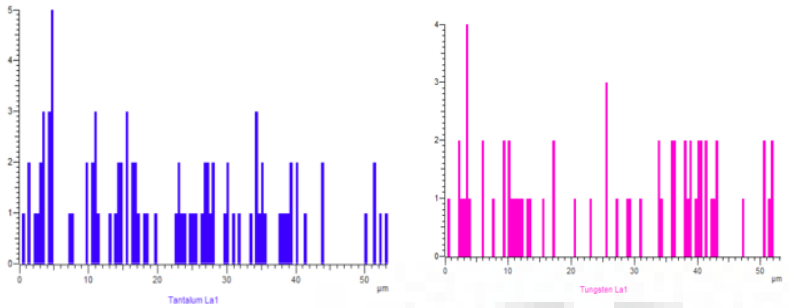

(g) Ta (h)W

Fig 4.10 Line analysis across the microstructure of S1 (a) BSE Image and Ka values of (b)Ti (c)C (d)N (e)Co (f)Ni (g)Ta (h)W.

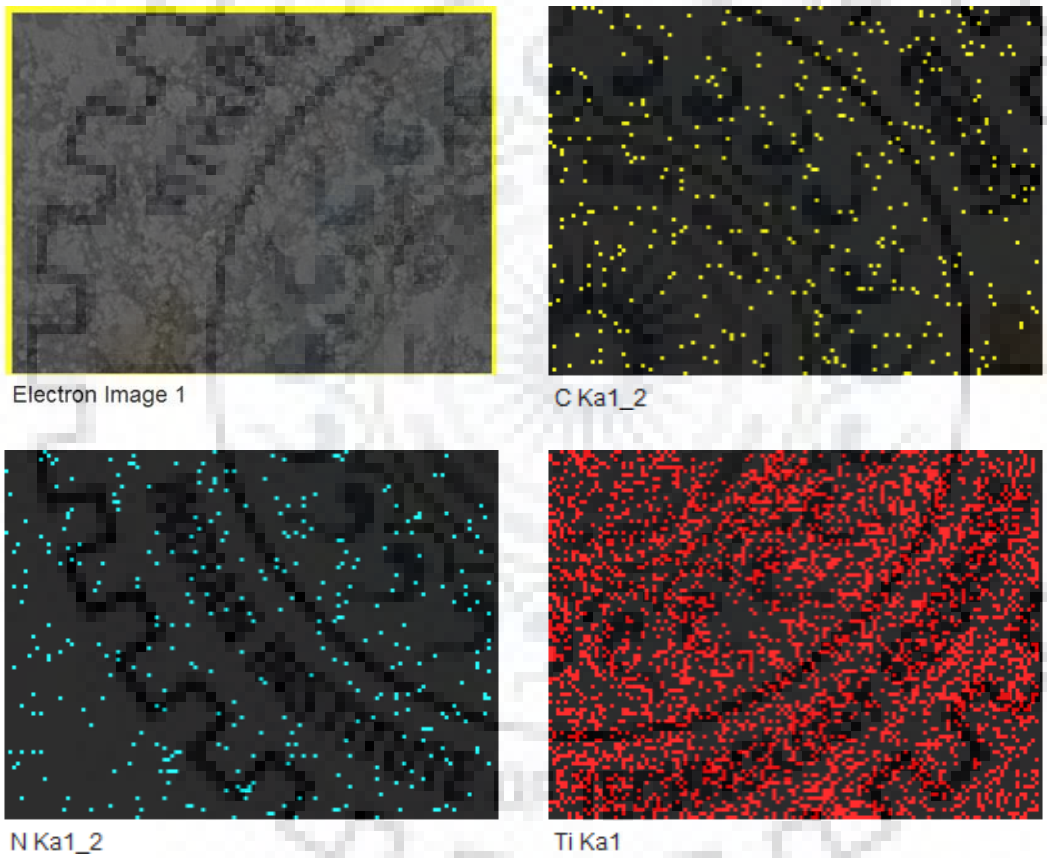

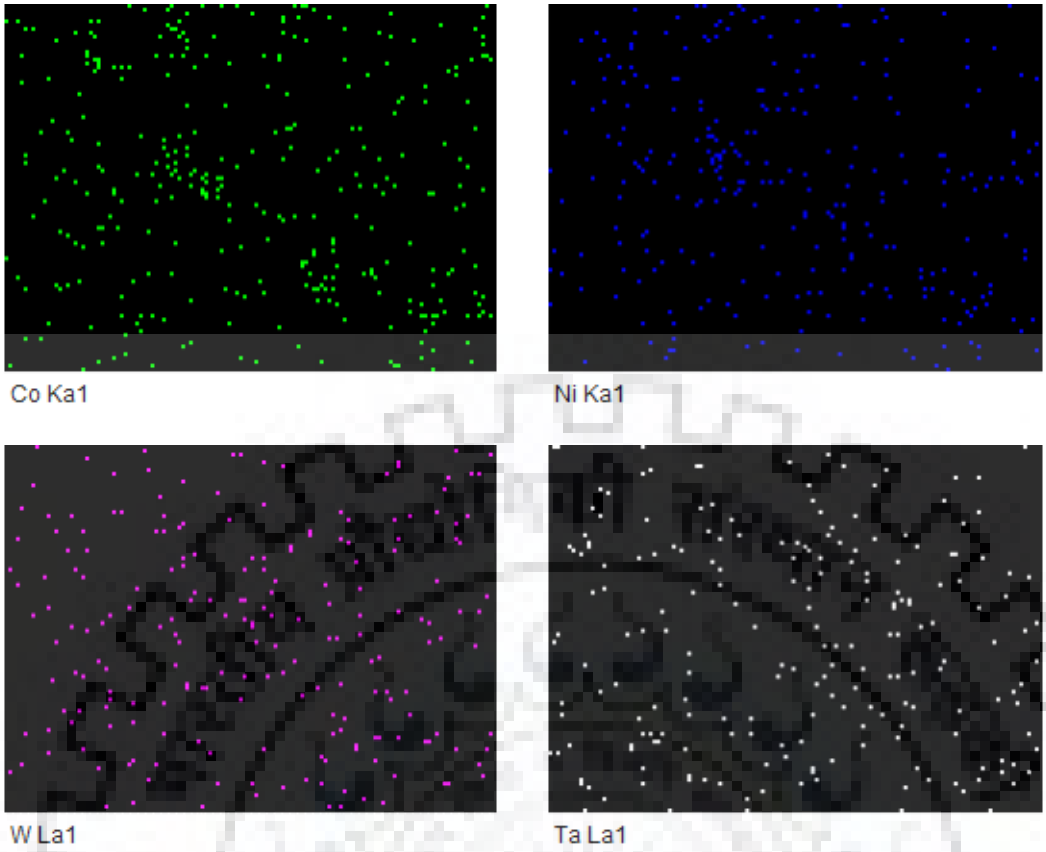

Fig 4.11 Elemental mapping of elements present in the sintered sample at 1200℃

The electron mapping shows at which position the concentration of element is higher, thereby helping us to locate the three phases (core, rim, binder).

4.4.3 Sample at 1300℃ (S2)

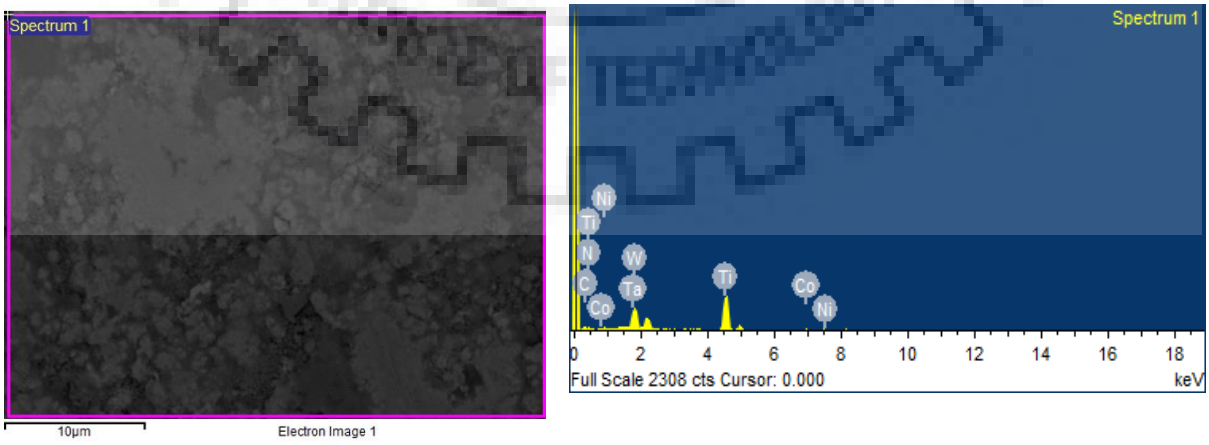

Fig 4.12 SEM and FESEM-BSE analysis of sample sintered at 1300℃

Element	Weight%	Atomic%
C K	5.51	19.74
N K	8.28	25.43
Ti K	45.47	40.84
Co K	5.01	3.66
Ni K	3.83	2.81
Ta M	14.86	3.53
W M	17.04	3.99
Totals	100.00	

Table 4.4 Show the weight percentage of elements present in the composition of S2

Line analysis and elemental mapping was done to determine the various phases which are formed after the sintering of the mixed powders.

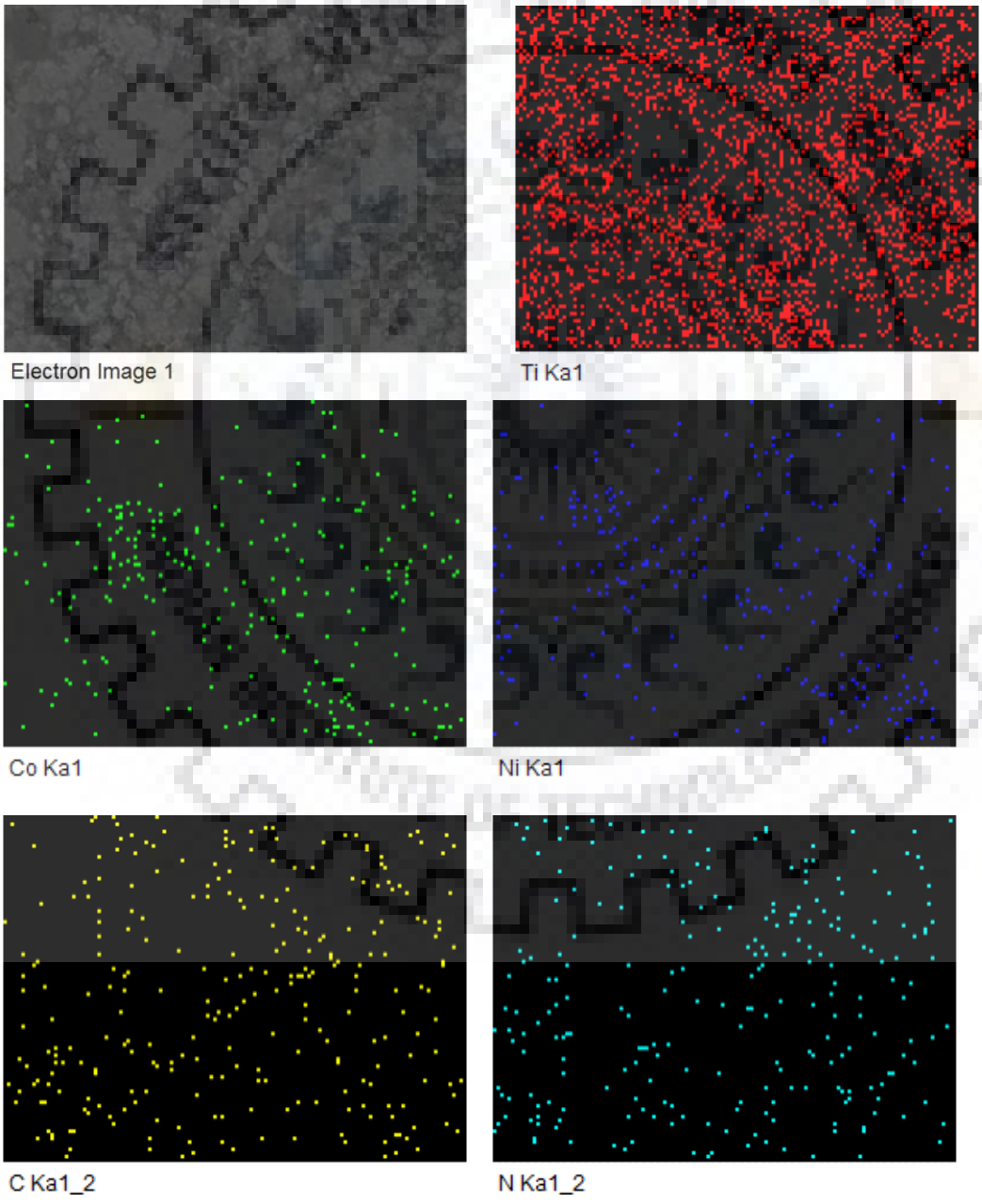

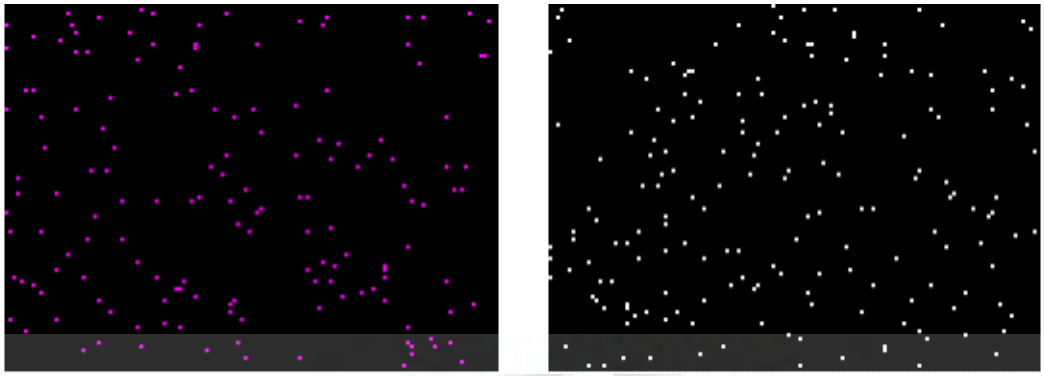

Fig 4.13 Elemental mapping of sample sintered at 1300℃ (S2)

Images for the line mapping are shown below.

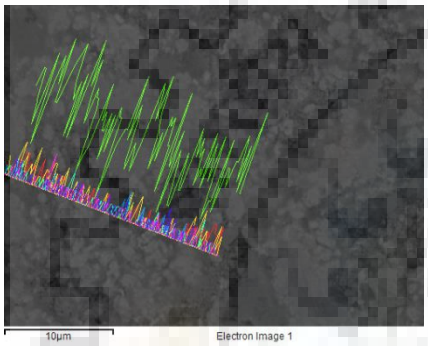

(a)

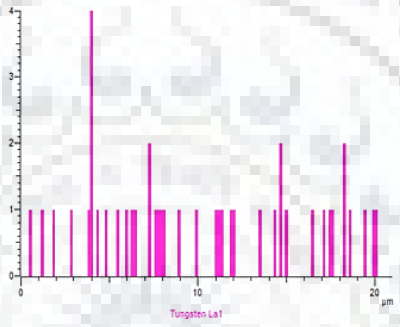

(b)W

(c)C

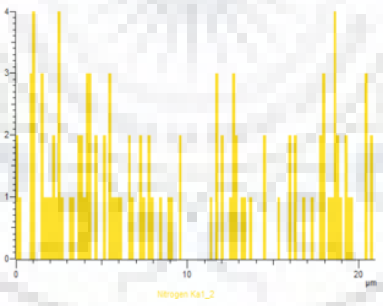

(d)N

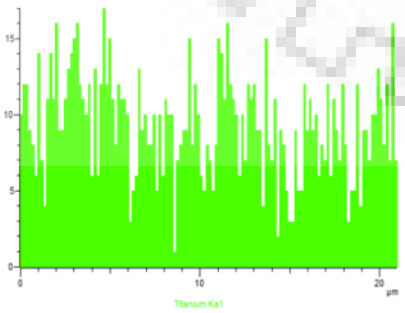

(e)Ti

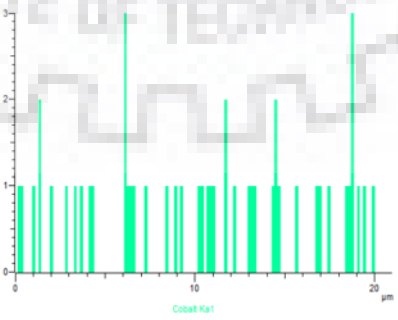

(f)Co

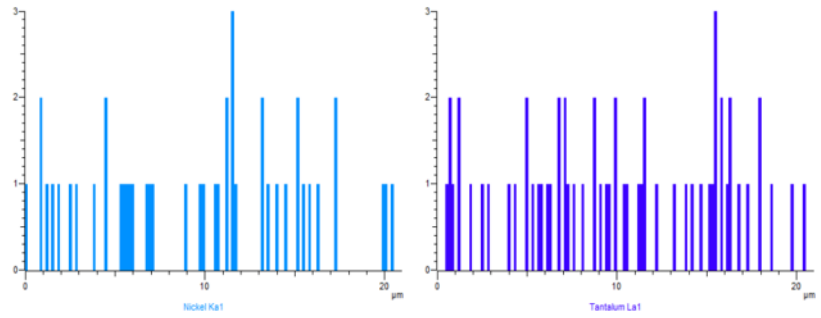

(g)Ni (h)Ta

Fig 4.14 Line mapping for sample S2 (a)BSE image for the are used for mapping and Ka values for (b)W (c)C (d)N (e)Ti (f)Co (g)Ni (h)Ta

4.4.4 Sample at 1350℃ (S3)

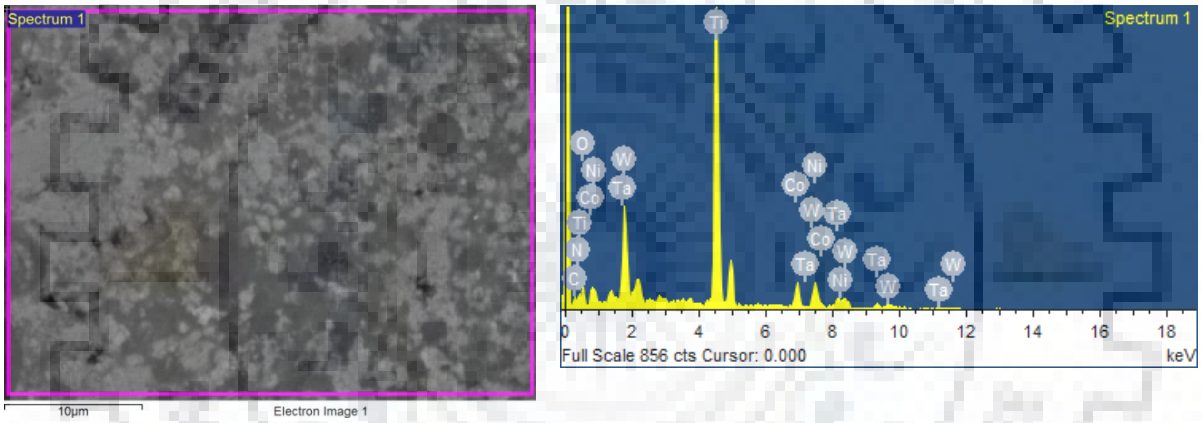

Fig 4.15 BSE and FESEM-EDS analysis of sintered sample at 1350℃

Element	Weight%	Atomic%
C K	10.12	27.83
N K	5.44	12.83
O K	9.57	19.77
Ti K	39.45	27.22
Co K	7.27	4.07
Ni K	8.31	4.68
Ta M	9.02	1.65
W M	10.82	1.95
Totals	100.00	

Table 4.5 Shows the weight percentage of elements present in S3

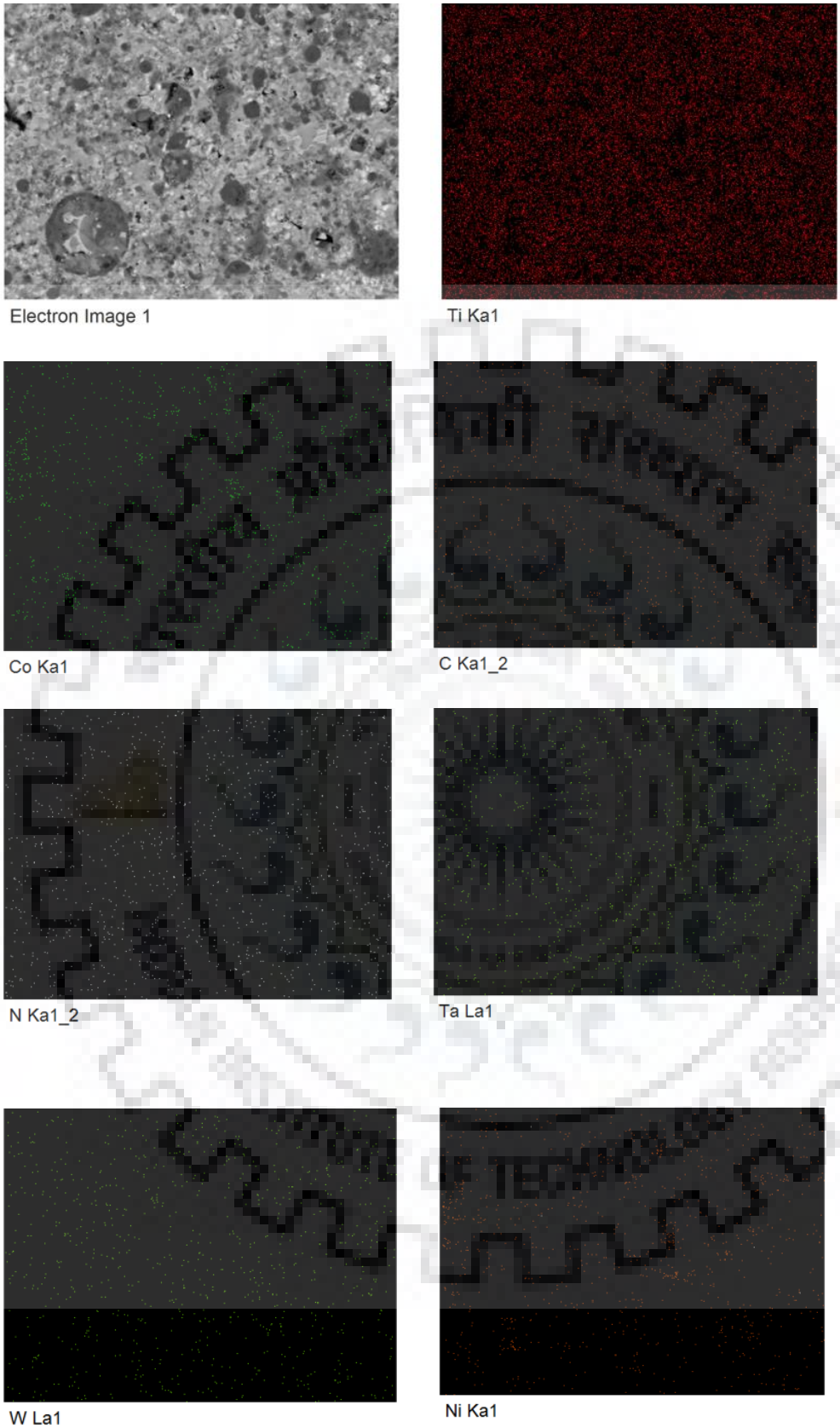

Fig 4.16 Elemental mapping of the sample S3

The elemental mapping reveals the presence of phases present in the sintered material and the line analysis reveals the phases that are produced after sintering. Images for line analysis are shown below.

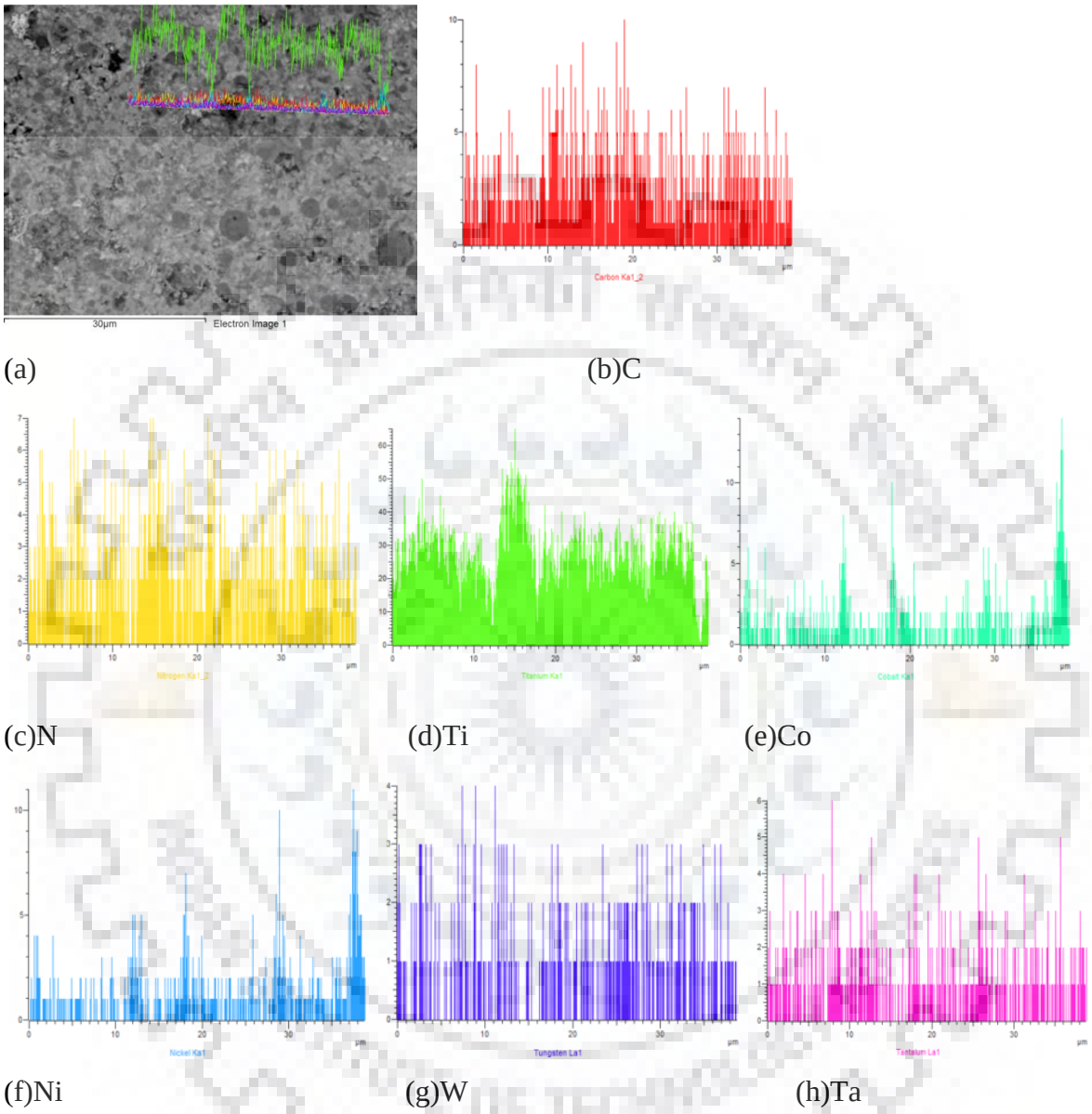

(a) (b)C

(c)N (d)Ti (e)Co

(f)Ni (g)W (h)Ta

Fig 4.17 Line analysis of the sample sintered at 1350℃ (a)BSE Image Ka values of (b)C (c)N (d)Ti (e)Co (f)Ni (g)W (h)Ta

4.4.5 Sample at 1500℃ (S4)

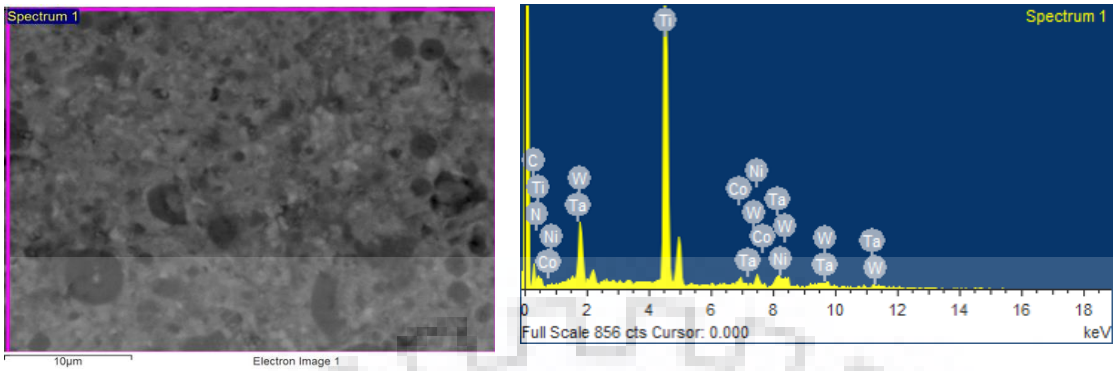

Fig 4.18 BSE and FESEM –EDS analysis of sample sintered at 1500℃

Table 4.6 The weight percentage of elements present in S4

Element	Weight%	Atomic%
C K	15.31	40.14
N K	7.73	17.38
Ti K	55.10	36.24
Co K	2.44	1.31
Ni K	4.37	2.34
Ta M	6.58	1.15
W M	8.47	1.45
Totals	100.00	

The BSE of the microstructure reveals the core rim phases but it shows very less concentration of binder phase. Also the thickness of the rim phase is more which is given due to solid solution re-precipitation control growth reaction or grain shape accommodation. The table 4.6 shows the weight distribution of the element present in the mixed powder.

Point analysis reveals the core, rim and binder phase in the microstructure. Line analysis and Elemental mapping reveals the presence of phases present in the matrix or the material after sintering. The images below shows the outcome that came after FESEM EDS analysis of Point analysis, Line analysis and Electron mapping.

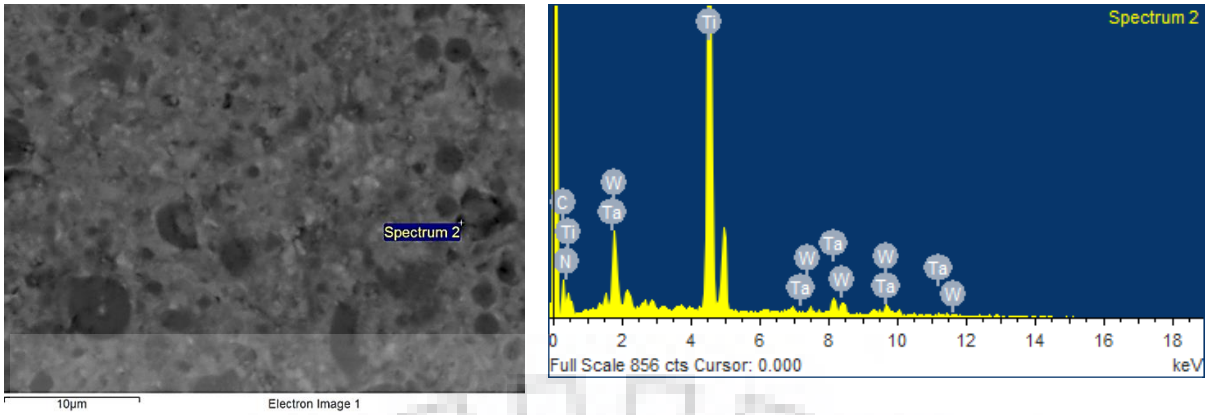

(a)

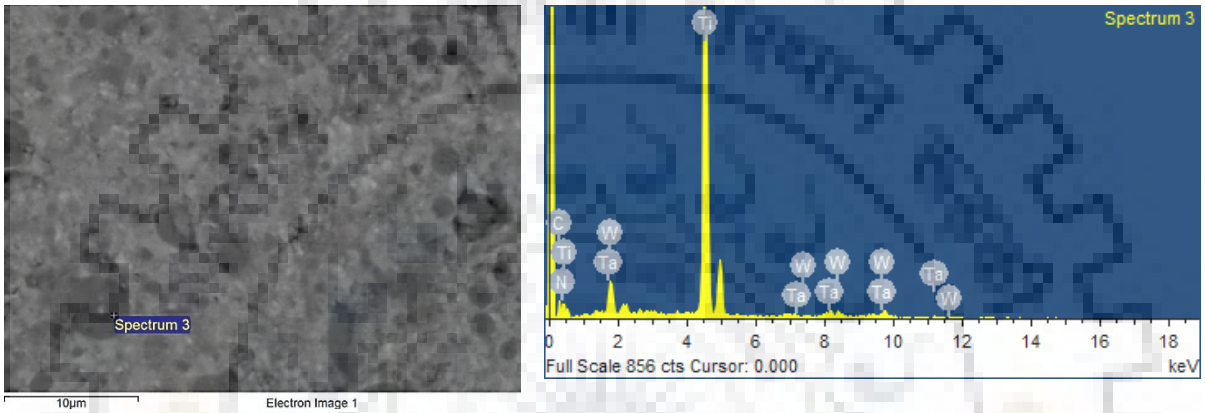

(b)

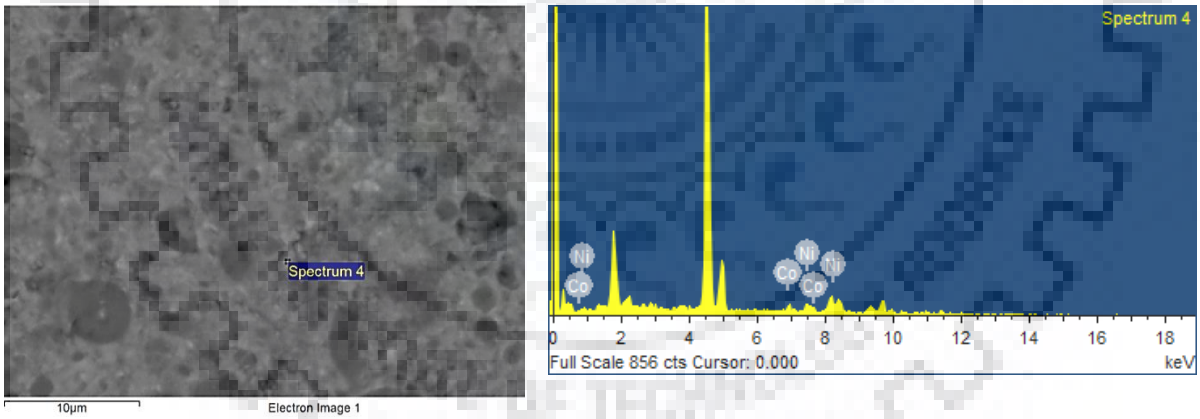

(c)

Fig 4.19 Shows the point analysis of S4 at different locations reveals the core, rim and binder phase. (a)spectrum 2 reveals core along with rim phase (b)spectrum 3 reveals rim phase (c)spectrum 4 reveals binder phase.

The line analysis along with elemental mapping serves to determine the phases which are present and the distribution of elements respectively.

Fig 4.20 Elemental mapping of sintered sample at 1500℃

Line analysis provides the data of the phases which are present in the microstructure, in conjugation with elemental mapping.

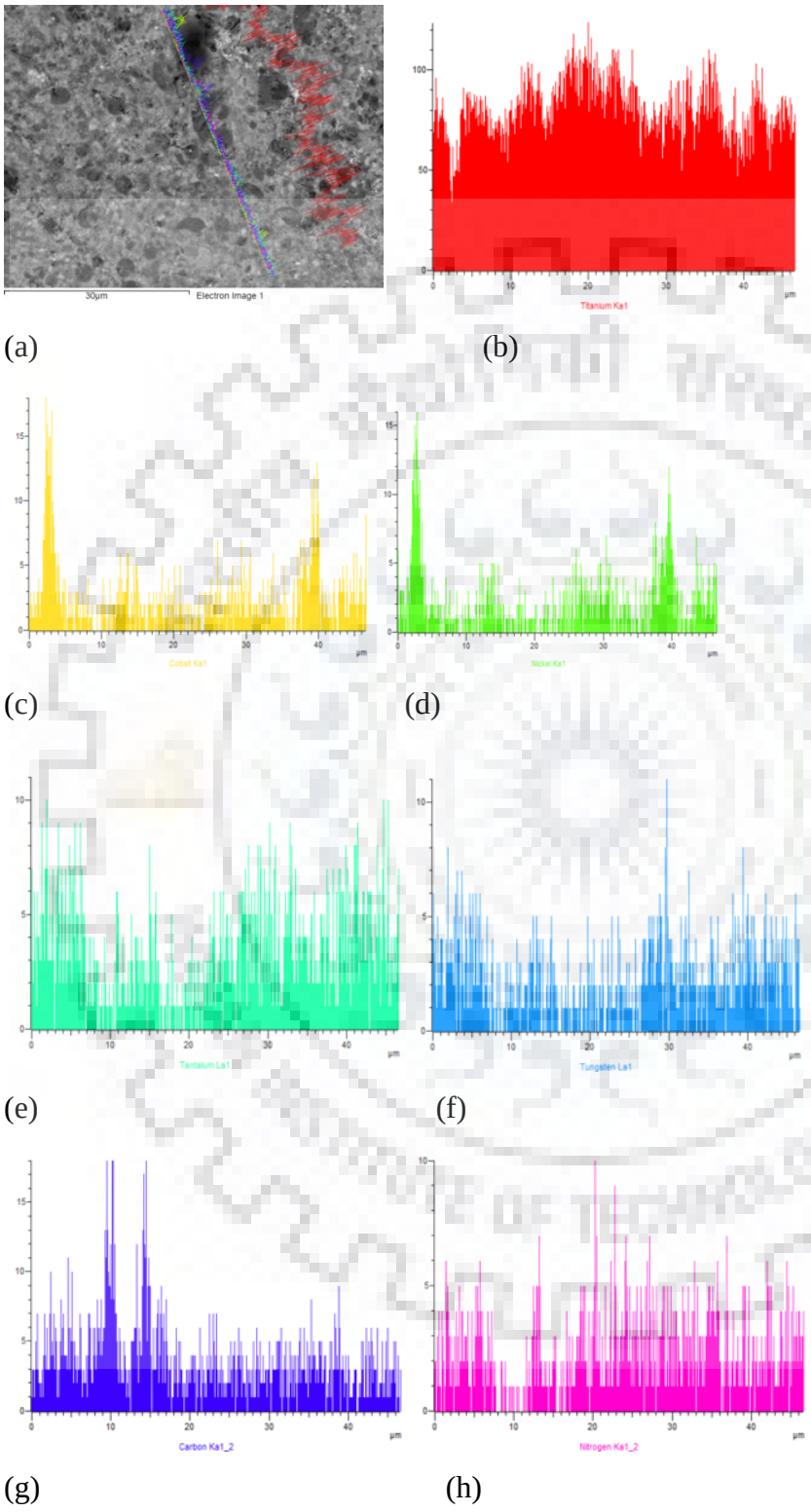

(a) (b)

(c) (d)

(e) (f)

(g) (h)

Fig 4.21 Line analysis of S4 (a)BSE image (b)Ti (c)Co (d)Ni (e)Ta (f)W (g)C (h)N

SEM analysis of the samples S3(1350℃) and S4(1500℃) was done to also determine the average grain size using linear intercept method and also with the help of ImageJ Analyzer. It was noted that as the sintering parameters changed the grain size decreased which in turn was the result of high grain shape accommodation factor which leads to excessive thickening of outer rim in S4.

Table 4.7 Designation, composition, heating rate, final temperature, relative density and average grain size of the processed cermets

Designation	Composition	Heating Rate(℃/ **min**)	Final Temperature(℃)	Relative density(%)	Carbide (core+rim) size ($\boldsymbol{\mu m}$)
S3	Ti(CN)-10wt%WC-10wt%TaC-10wt%Ni-10wt%Co	100	1350	94.6	$2.6 \pm \mathbf{0.3}$
S4	Ti(CN)-10wt%WC-10wt%TaC-10wt%Ni-10wt%Co	600	1500	95.8	$1.8 \pm \mathbf{0.1}$

4.5 Mechanical properties

The mechanical properties were calculated using Vickers Hardness Indenter and the Fracture toughness was measured. The hardness and fracture toughness value changed as the sintering parameters were changed to produce a dense material.

Table 4.8 Values for hardness and fracture toughness

Sample	Vickers Hardness (GPa)	Fracture Toughness (MPa$\sqrt{\boldsymbol{m}}$)
S3 (1350℃)	10.79 ±0.18	6.51 ±0.11
S4 (1500℃)	16.11 ±0.16	7.70 ±0.14

The difference in the hardness and the fracture toughness for both the sample arises due to the fact that the grain size differs for them a lot. As the sintering parameters are changed the particle size decreases resulting in a compact and dense material. The decrease in the particle size leads to a huge change in the hardness and the fracture toughness. The hardness of S4 is nearly 33% more than the hardness value of S3. Also the fracture toughness is different, higher for S4 as compared to S3.

The hardness and fracture toughness was calculated using an optical microscope and then with SEM to determine its value. The images for both samples are attached below.

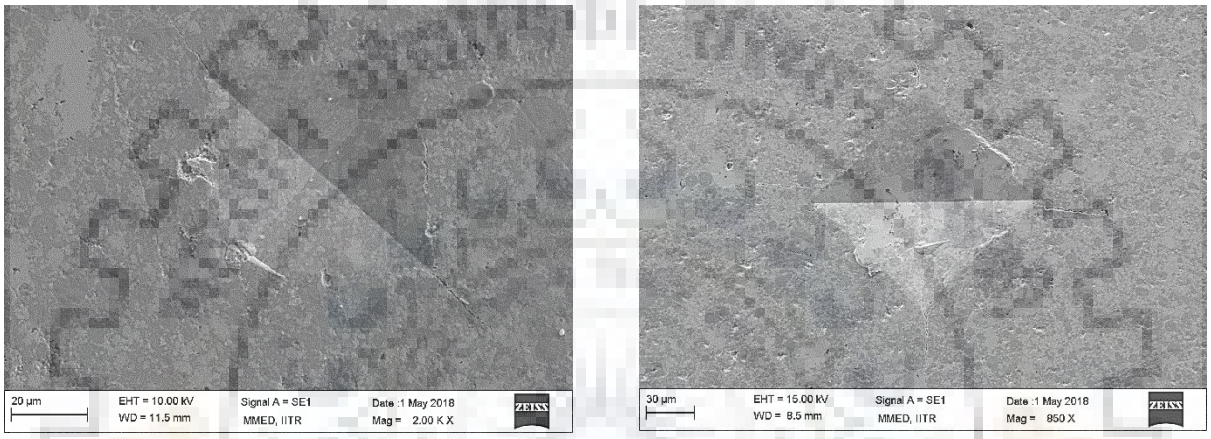

(a)

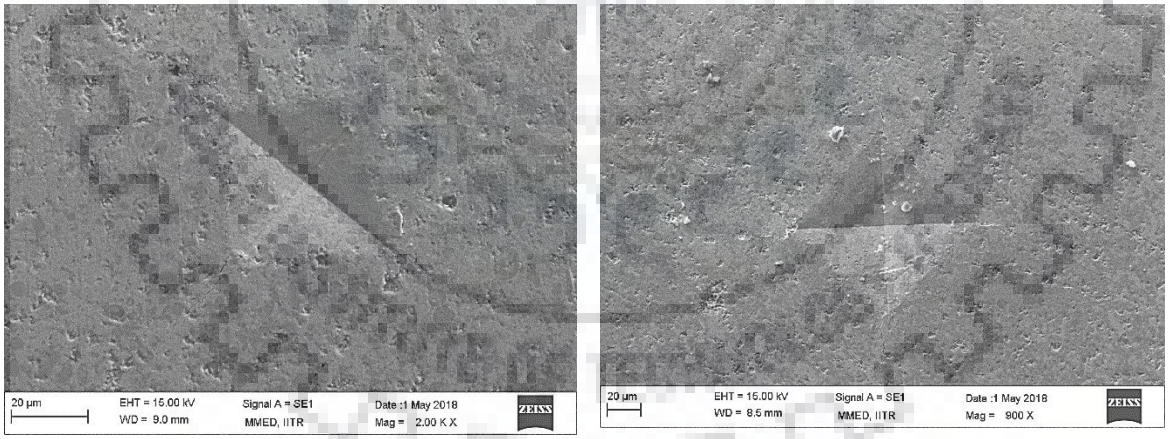

(b)

Fig 4.22 Indentation measurement and Crack length measurement from SEM for (a)S3 and (b)S4

4.6 Fracture morphology

The SEM analysis of the fracture surface reveals the fracture occurring here is of mixed nature i.e. it shows both trans-granular and intra-granular grain fracture Absence of dimples shows that the fracture is of brittle nature, which is due to the fact that the given sample have ceramic nature.

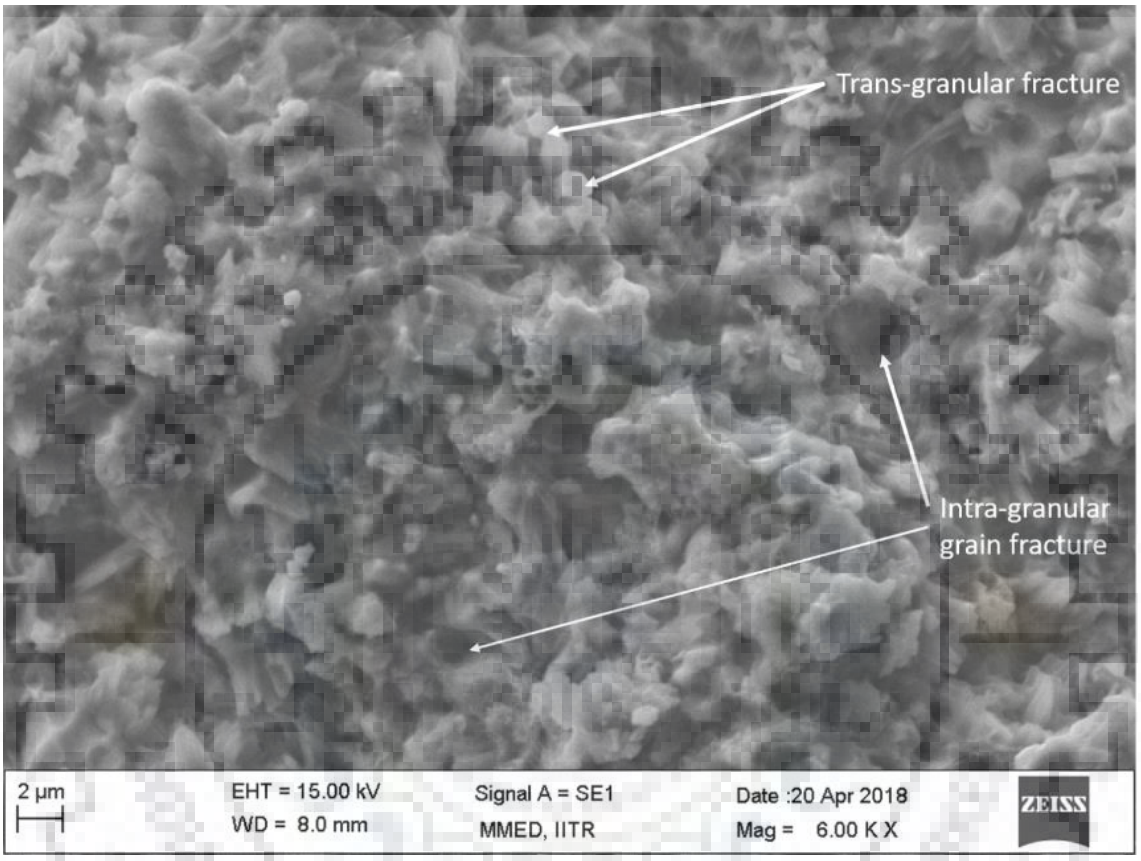

Fig 4.23 SEM images of fracture surfaces shows the intra-granular grain fracture and trans-granular fracture

The trans-granular grain fracture is indicated by the fracture that occurs along the grain boundary while intra-granular grain fracture occurs within the grain. In the Fig 4.33 the fracture is shown.

4.7 Sliding wear

Sliding wear was done to determine the wear characteristics of the material. After determining the hardness and fracture toughness, the sample was taken for sliding wear on a ball and disc sliding machine and the coefficient of friction was calculated from the graph after conducting three test per sample. Ball used was WC-Co.

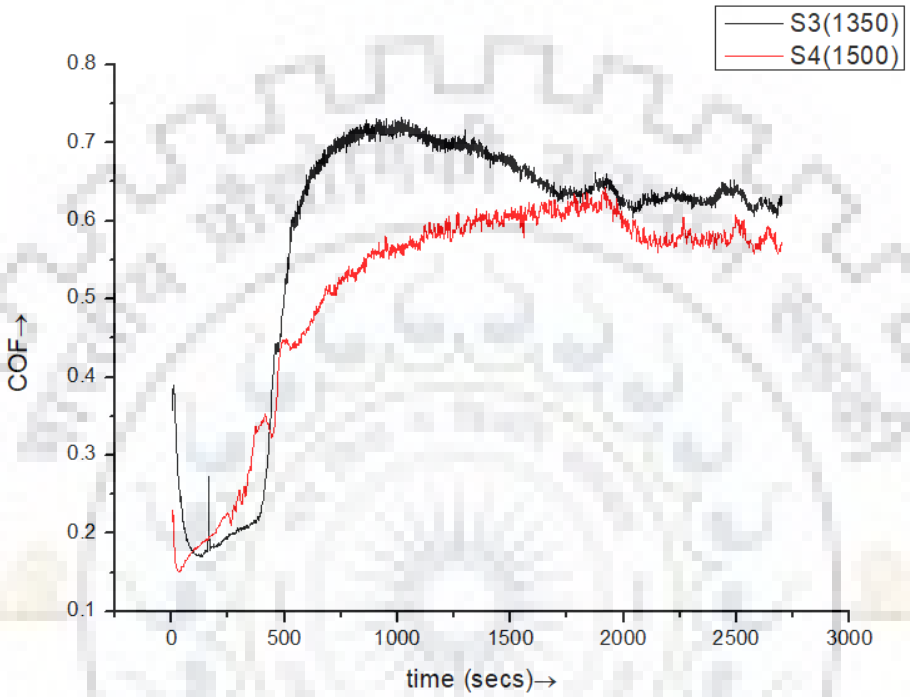

Fig 4.24 COF graphs for samples underwent Sliding Test, relative humidity 32%

Profilometer was done to determine the depth and width of the wear track after sliding wear test. This was also done to determine the wear volume of the materials. Graphs for two samples are shown below.

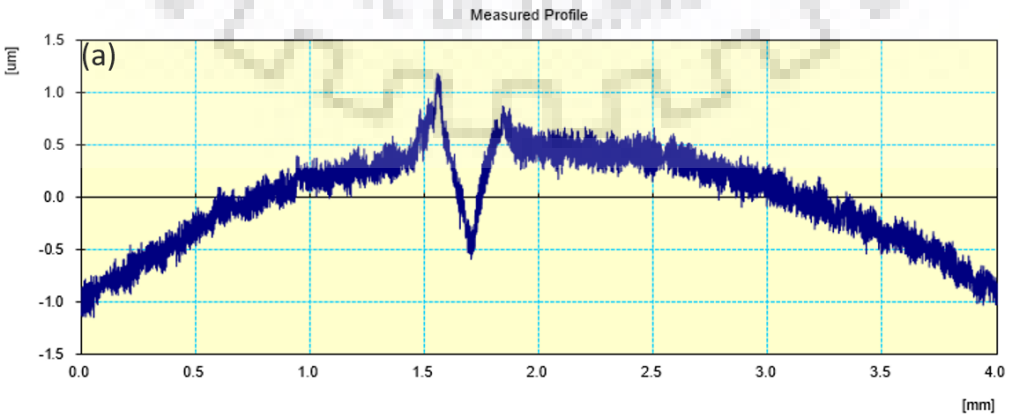

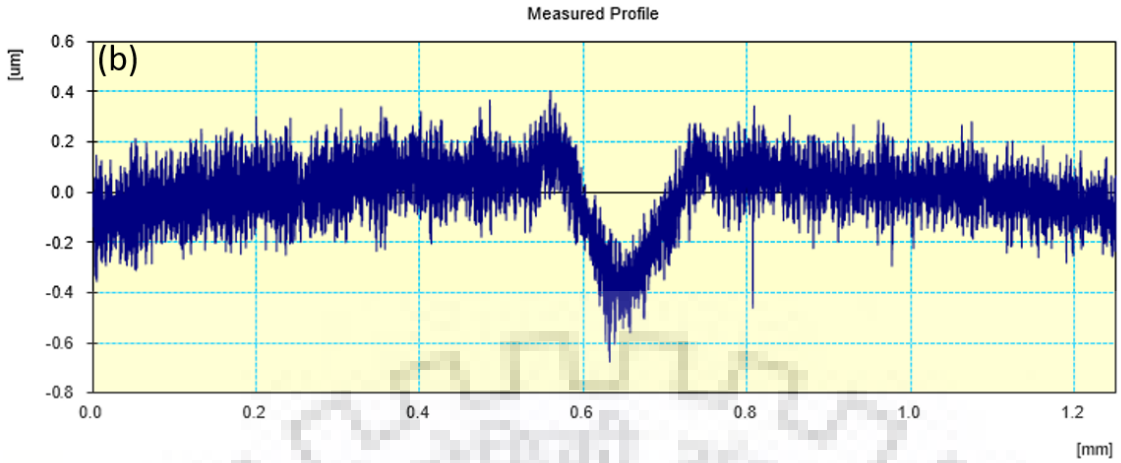

Fig 4.25 Typical Surface roughness profile of TiCN-TaC-WC-Co-Ni material sintered at (a)1350℃ (b)1500℃

Surface roughness profile helped in determining the wear volume of the samples after sliding wear.

Table 4.9 Wear volume and average grain size for Carbide(core+rim) for sintered cermets

Cermet	Wear Volume ($x10^{-3}$ mm^3)	Hardness (GPa)	Fracture toughness (MPa$\sqrt{\mathbf{m}}$)	Carbide(core+rim) size (**μm**)
S3	3.91±0.15	10.79±0.18	6.515±0.11	2.6±0.3
S4	1.04±0.39	16.11±0.16	7.704±0.14	1.8±**0. 1**

4.8 Wear surface analysis

The worn surface of the sample and the WC-Co balls was subjected to SEM analysis to determine the changes in the composition along with the SEM analysis of the debris that was produced after the wear test. Oxide formation was evident after FESEM EDS analysis of the wear surface of the sample.

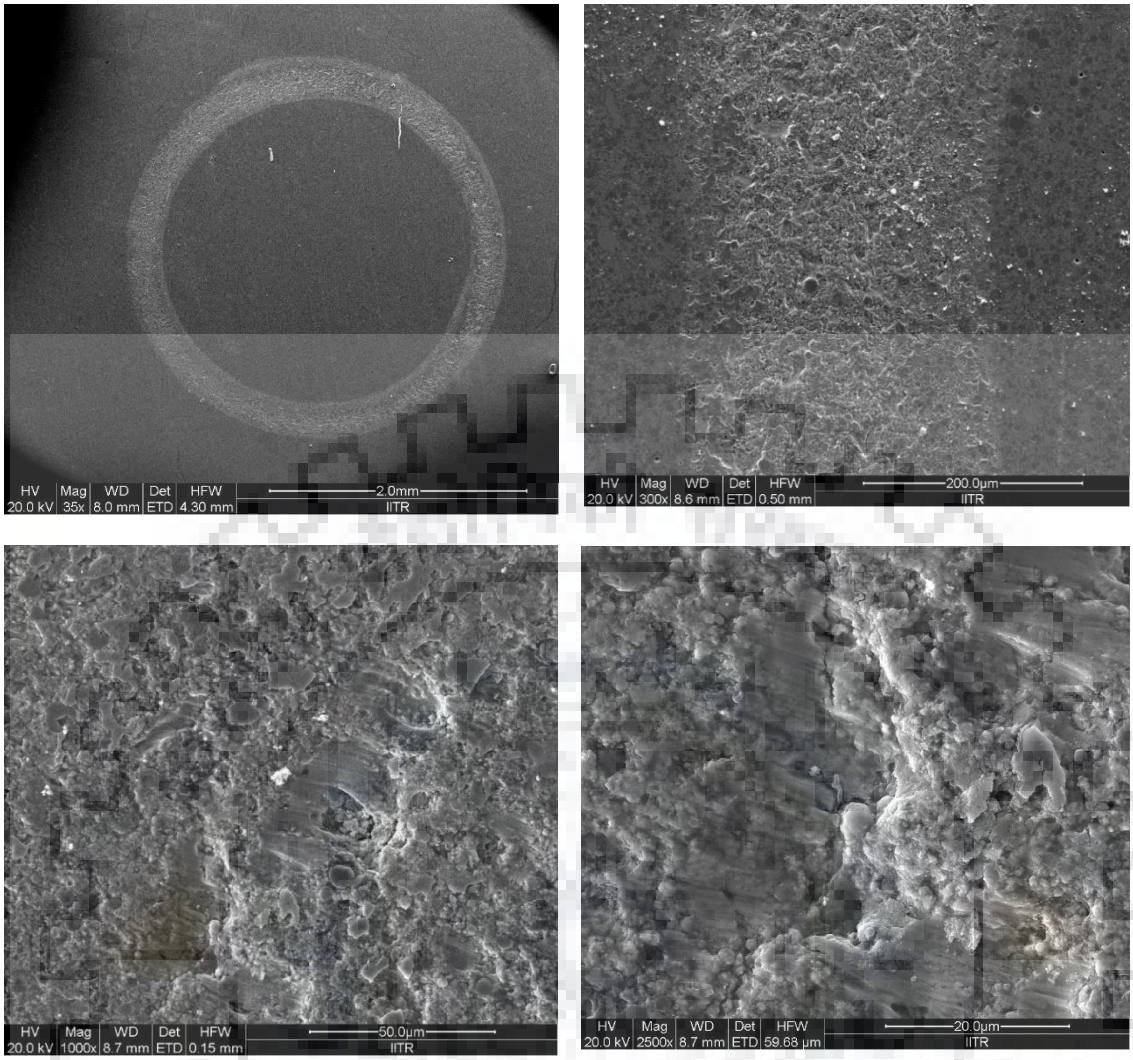

Fig 4.26 SEM images for the wear surface of S3 showing the surface morphology of the sample after sliding wear.

In the above images, it can be clearly seen that the sample is easily worn out. This is due to the fact that the WC-Co balls are harder as compared to the sintered sample S3. Thus the wear is more. The fracture mechanism that accompanies here is the intra-granular grain fracture. Also there is grain pull out and ploughing occurring which can be clearly seen from the SEM images, suggesting that the material binder phases is softer and thus won't be able to withstand high speed abrasion.

The EDS analysis of the wear track reveals the formation of oxide on the surface of the material which is evident from the plot shown below

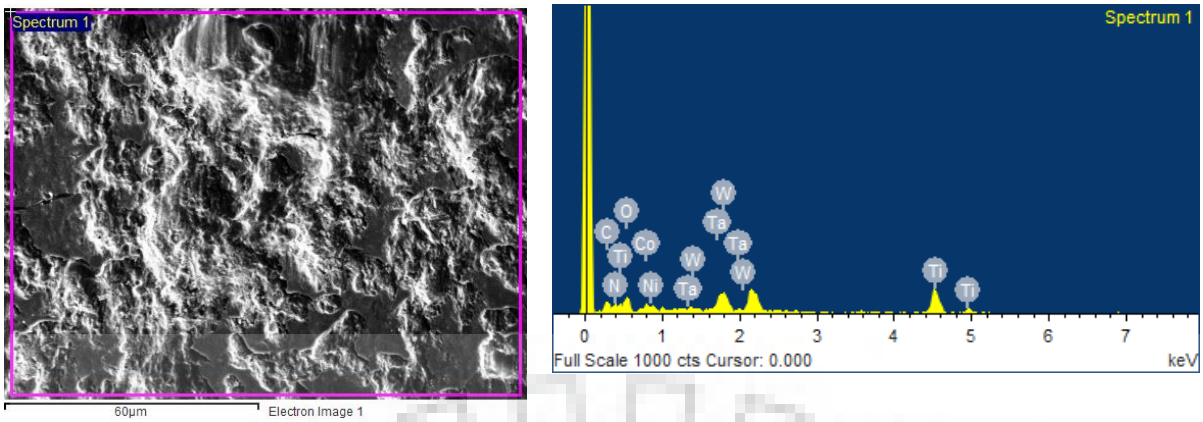

Fig 4.27 SEM images for the wear track and the FESEM EDS analysis of the wear track of S3

Element	Weight%	Atomic%
C K	4.97	15.99
N K	2.07	5.72
O K	11.68	28.21
Ti K	40.83	32.92
Co L	12.38	8.12
Ni L	6.98	4.59
Ta M	9.20	1.96
W M	11.88	2.50
Totals	100.00	

Table 4.10 Weight percentage of various elements present in the material after sliding wear test of S3

The FESEM EDS reveals the formation of oxide on the surface which is due to high speed abrasion from the WC-Co balls. The Table 4.10 shows that the oxide content is more and it is only present in the wear track region and not on anywhere else on the cermet material.

SEM images for the debris reveals, the debris particles are not fine in size, which can be seen from the images below.

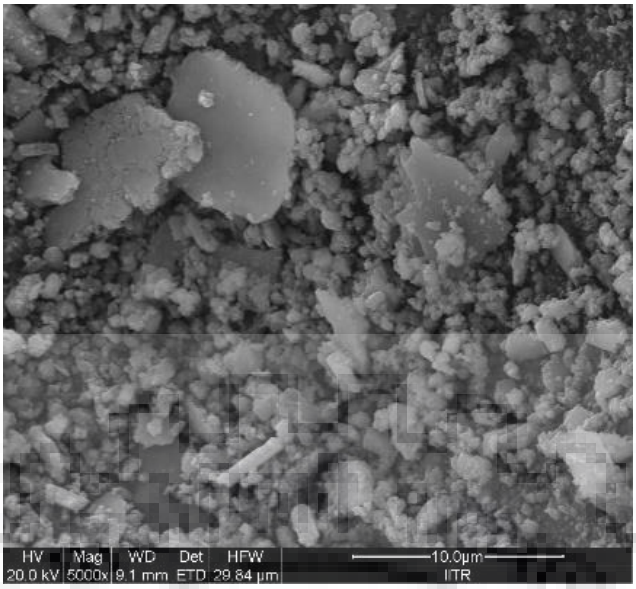

Fig 4.28 SEM image of the debris collected after sliding wear of sample S3

The chipping is due to the high hardness of WC-Co balls as compared to S3. Also this resulted in a large sized debris and the average debris particle size is around 4micron.

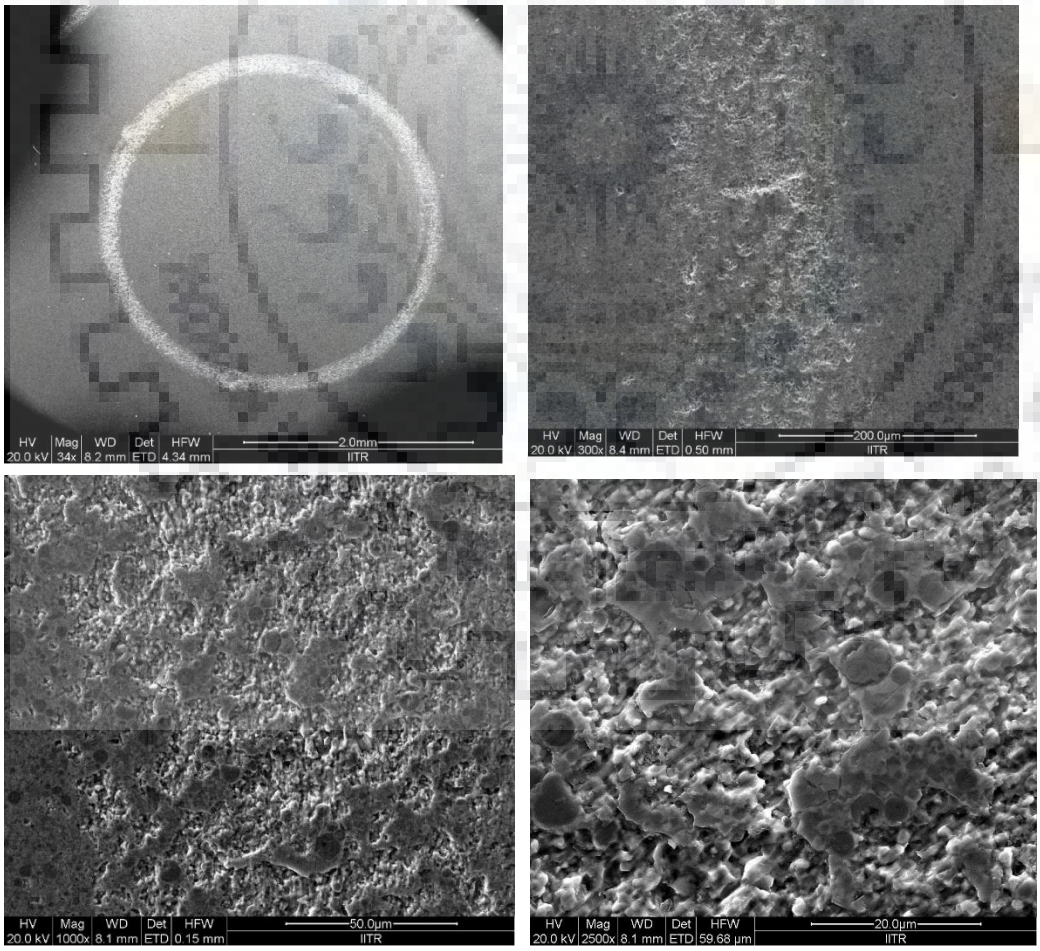

Fig 4.29 SEM images for the wear track, and eroded surfaces revealing remnant of the phases left after wear for S4

In Fig 4.29 the dark phases shown are your core rim structure which has been confirmed by the FESEM EDS analysis. This phase is shown due to the remnant of the phases left behind after the removal of the binder phase. As the binder phase is soft, WC-Co balls easily erodes the surfaces leaving behind the core-rim phase thus making it unsuitable for high speed abrasive applications. Due to decrease in the grain size the hardness of S4 increase and is nearly equivalent to the WC-Co balls thus resulting in less wear during sliding wear test. The EDS analysis of the wear track surface and the dark phases are shown below.

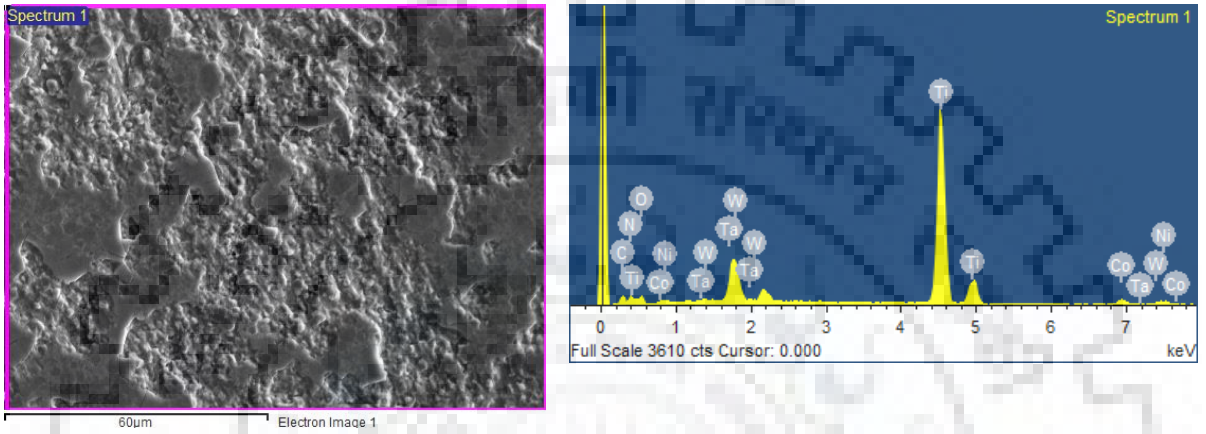

(a)

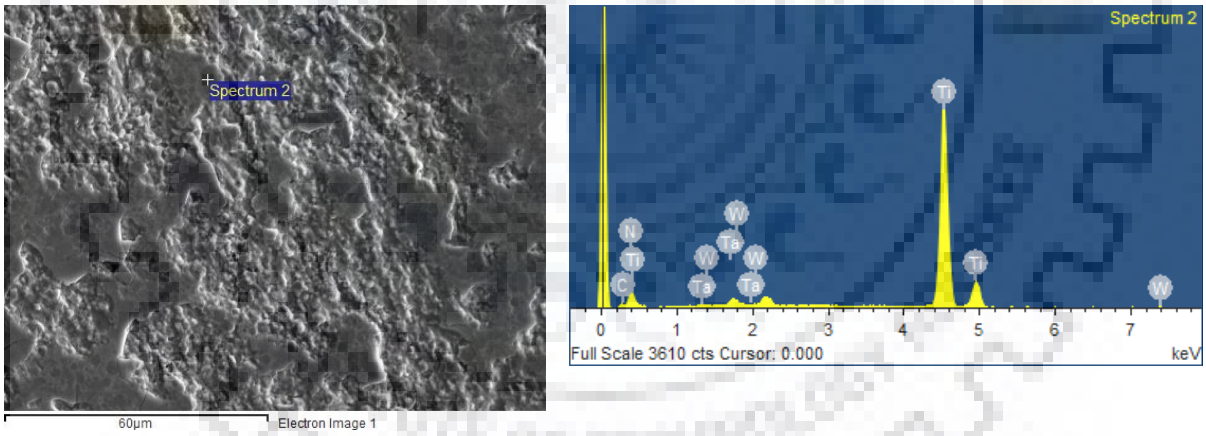

(b)

Fig 4.30 FESEM EDS analysis of the S4 (a)wear track (b)dark phase/region

Element	Weight%	Atomic%
C K	6.06	18.47
N K	2.31	6.03
O K	11.68	26.71
Ti K	54.03	41.25
Co K	2.89	1.79
Ni K	2.68	1.67
Ta M	10.90	2.20
W M	9.45	1.88
Totals	100.00	

Table 4.11 Weight percentage for Fig 4.30(a)

Element	Weight%	Atomic%
C K	2.30	6.82
N K	12.60	32.10
Ti K	80.92	60.26
Ta M	3.52	0.69
W M	0.67	0.13
Totals	100.00	

Table 4.12 Weight percentage for Fig 4.30(b)

The above EDS analysis confirms that the binder phase being soft was eroded easily but the wear was not much due to high hardness of the S4, due to decrease in grain size due to change of sintering parameters which in turn led to more grain shape accommodation. The elemental mapping was done to determine the distribution of the elements and also the presence of oxide layer on the sample.

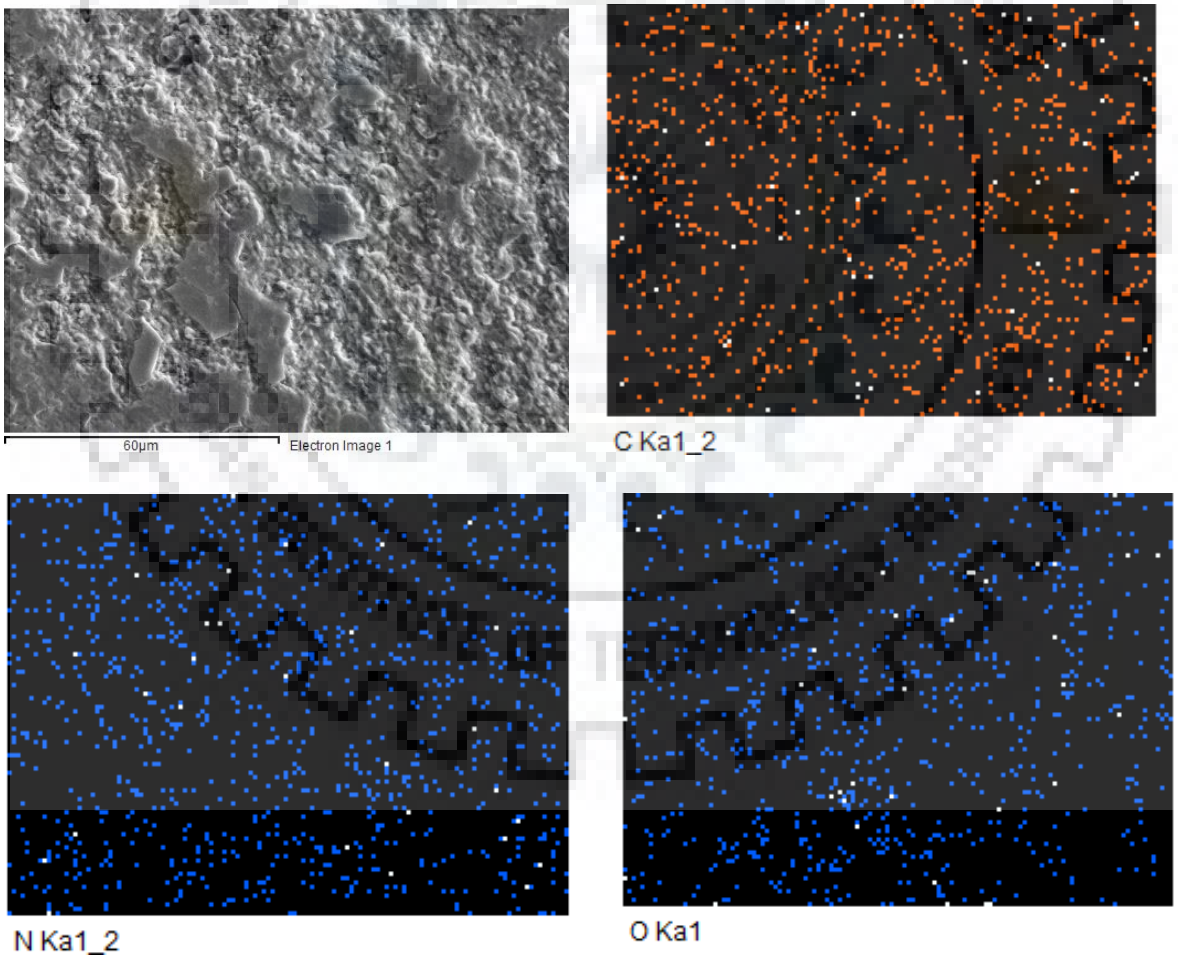

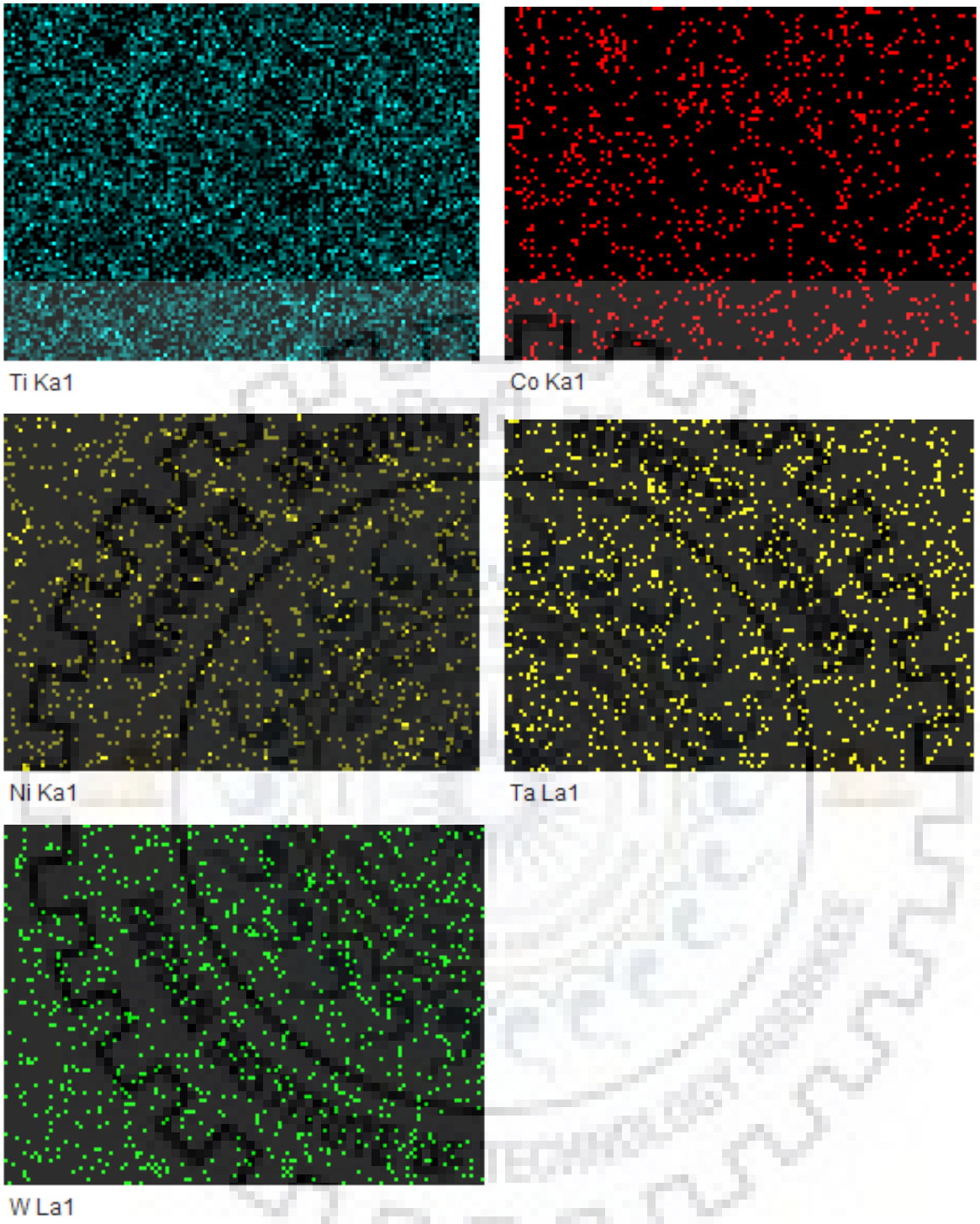

Fig 4.31 Elemental mapping reveals the presence of oxide layer only on the wear tracks of S4

The elemental mapping shows that the oxide layer is only present on the wear tracks that is on the eroded surface.

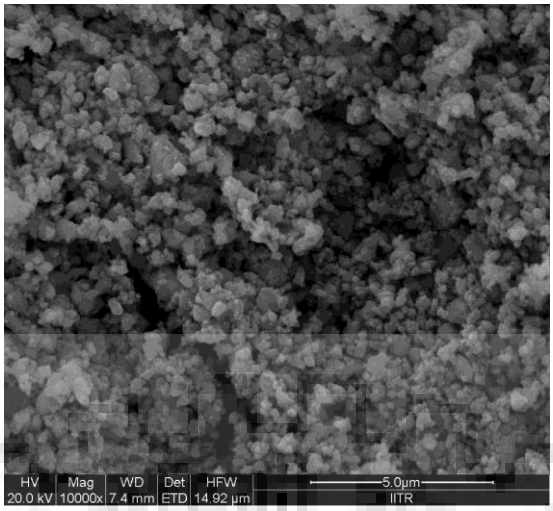

Fig 4.32 SEM images for the debris from S4 sliding wear test

SEM images of the debris was taken and it showed very fine sized particles which confirms the fact that the wear was minimal.

Cermets with the composition of Ti(CN)-10wt%WC-10wt%TaC-10wt%Ni-10wt%Co was prepared by spark plasma sintering at 40 MPa for 3 min in argon atmosphere at 1200℃, 1300℃, 1350℃ and 100℃/$\boldsymbol{min}$ heating rate, and 1500ºC at 600ºC/min. The relative density changed from 94.6% and 95.8%. The carbide (core+rim) size changed from 2.6 micron to 1.8 micron. The change in microstructure is related to the grain shape accommodation which led to spheroidal grain shapes.

The hardness for the sample sintered at 1350ºC at 100ºC/min and 1500ºC/min at 600ºCmin are 10.79GPa and 16.11GPa respectively and fracture toughness are 6.51 MPa$\sqrt{\boldsymbol{m}}$ and 7.70 MPa$\sqrt{\boldsymbol{m}}$ respectively. There has been a 44% reduction in carbide size due to change in sintering parameters which in turn has resulted in a 33% increase in hardness value and 15% increase in the fracture toughness value. The wear volume for the both samples were calculated to be $3.91x10^{-3}$ mm^3 and $1.04x10^{-3}$ mm^3 respectively, which shows there has been a 74% reduction in the wear volume. This also indicates that the microstructure plays an integral role in the mechanical properties of these cermets. During sliding the binder phase is deformed followed by the fracture of the core and rim phases.

- The sintering parameters can be changed to make a more dense material while keeping in mind the leakage problem which might arises due to high temperature.
- The microstructure of the sample can be further investigated as it showed spheroidal shapes instead of polyhedral shapes as per the literature.
- The changes which accompanies in mechanical properties due to microstructural changes can be further investigated to determine a harder material with the same composition.
- Further analysis on the mechanical properties of this composition material can be done to determine its application either for high speed machining tools or for high temperature material uses.

REFERENCES

[1] Alida Bellosi, Valentina Medri, and Frederic Monteverde, "Processing and Properties of Ti(C,N)- WC Based Materials", *J. Am. Ceram. Soc. 84[11]2669-76 (2001).*

[2] S. Zhang, "Titanium carbonitride-based cermets: processes and properties," *Mater. Sci. Eng. A*, vol. 163, no. 1, pp. 141–148, 1993.

[3] N. Liu, C. Han, Y. Xu, S. Chao, M. Shi, and J. Feng, "Microstructures and mechanical properties of nanoTiN modified TiC-based cermets for the milling tools," *Mater. Sci. Eng. A*, vol. 382, no. 1, pp. 122–131, 2004

[4] K. Yang, Q. Yang, and Y. F. Bao, "Formation of carbonitride precipitates in hardfacing alloy with niobium addition," *Rare Met.*, vol. 32, no. 1, pp. 52–56, 2013.

[5] S. Kang, "Some issues in Ti(CN)-WC-TaC cermets," *Mater. Sci. Eng. A*, vol. 209, no. 1, pp. 306–312, 1996.

[6] N. Liu, S. Chao, and H. Yang, "Cutting performances, mechanical property and microstructure of ultra-fine grade Ti(C,N)-based cermets," *Int. J. Refract. Met. Hard Mater.*, vol. 24, no. 6, pp. 445–452, 2006.

[7] L. Karlsson, L. Hultman, M. P. Johansson, J.-E. Sundgren, and H. Ljungcrantz, "Growth, microstructure, and mechanical properties of arc evaporated TiCxN1−x (0≤x≤1) films," *Surf. Coatings Technol.*, vol. 126, no. 1, pp. 1–14, 2000

[8] M. G. Gee, B. Roebuck, P. Lindahl, and H.-O. Andren, "Constituent phase nanoindentation of WC/Co and Ti(C,N) hard metals," *Mater. Sci. Eng. A*, vol. 209, no. 1, pp. 128–136, 1996

[9] S. Ahn and S. Kang, "Formation of Core / Rim Structures in Ti (C , N) -WC-Ni Cermets via a Dissolution and Pricipitation Process," *J. Am. Ceram. Soc.*, vol. 83, pp. 1489–1494, 2000.

[10] S. Kang, "Some issues in Ti(CN)-WC-TaC cermets," *Mater. Sci. Eng. A*, vol. 209, no. 1, pp. 306–312, 1996.

[11] S. Ahn and S. Kang, "Formation of Core / Rim Structures in Ti (C , N) -WC-Ni Cermets via a Dissolution and Pricipitation Process," *J. Am. Ceram. Soc.*, vol. 83, pp. 1489–1494, 2000.

[12] X. Shangzhi, W. Huiping, and Z. Shuzhu, "The influence of TiN content on properties of Ti(CN) solid solution," *Mater. Sci. Eng. A*, vol. 209, no. 1, pp. 294–297, 1996.

[13] E. Chicardi, J. M. Córdoba, M. J. Sayagués, and F. J. Gotor, "Inverse core–rim microstructure in (Ti,Ta)(C,N)-based cermets developed by a mechanically induced self-sustaining reaction," *Int. J. Refract. Met. Hard Mater.*, vol. 31, pp. 39–46, 2012.

[14] Y. Peng, H. Miao, and Z. Peng, "Development of TiCN-based cermets: Mechanical properties and wear mechanism," *Int. J. Refract. Met. Hard Mater.*, vol. 39, 2013.

[15] N. Liu, X. Liu, X. Zhang, and L. Zhu, "Effect of carbon content on the microstructure and mechanical properties of superfine Ti(C, N)-based cermets," *Mater. Charact.*, vol. 59, no. 10, pp. 1440–1446, 2008.

[16] Y. Zhang, Y. Zheng, J. Zhong, Q. Yuan, and P. Wu, "Effect of carbon content and cooling mode on the microstructure and properties of Ti(C,N)-based cermets," *Int. J. Refract. Met. Hard Mater.*, vol. 27, no. 6, pp. 1009–1013, 2009.

[17] J. Zackrisson, A. Larsson, and H.-O. Andrén, "Microstructure of the Ni binder phase in a TiC–Mo2C–Ni cermet," *Micron*, vol. 32, no. 8, pp. 707–712, 2001.

[18] A. Rajabi, M. J. Ghazali, J. Syarif, and A. R. Daud, "Development and application of tool wear: A review of the characterization of TiC-based cermets with different binders," *Chem. Eng. J.*, vol. 255, pp. 445–452, 2014.

[19]S. Zhou, W. Zhao, and W. Xiong, “Microstructure and properties of the cermets based on Ti(C,N),” *Int. J. Refract. Met. Hard Mater.*, vol. 27, no. 1, pp. 26–32, 2009.

[20]J. Wang, Y. Liu, P. Zhang, J. Ye, and M. Tu, “Effect of VC and nano-TiC addition on the microstructure and properties of micrometer grade Ti(CN)-based cermets,” *Mater. Des.*, vol. 30, no. 6, pp. 2222–2226, 2009.

[21]Y. Wang, S. Shu, F. Qiu, D. Zhou, J. Wang, and Q. Jiang, “Effect of W content on the compression properties and abrasive wear behavior of the (TiB2–TiCxNy)/(Ni+W) composites,” *Mater. Des.*, vol. 45, pp. 286–291, 2013.

[22]X. Chen, W. Xiong, J. Qu, Q. Yang, Z. Yao, and Y. Huang, “Microstructure and mechanical properties of (Ti,W,Ta)C-xMo-Ni cermets,” *Int. J. Refract. Met. Hard Mater.*, vol. 31, pp. 56–61, 2012.

[23]L. Chen, W. Lengauer, P. Ettmayer, K. Dreyer, H. W. Daub, and D. Kassel, “Fundamentals of liquid phase sintering for modern cermets and functionally graded cemented carbonitrides (FGCC),” *Int. J. Refract. Met. Hard Mater.*, vol. 18, no. 6, pp. 307–322, 2000.

[24]J. Xiong, Z. Guo, B. Shen, and D. Cao, “The effect of WC, Mo2C, TaC content on the microstructure and properties of ultra-fine TiC0.7N0.3 cermet,” 2007.

[25]W. Jun, L. Ying, Z. Ping, P. Jiancai, Y. Jinwen, and T. Minjing, “Effect of WC on the microstructure and mechanical properties in the Ti(C0.7N0.3)–xWC–Mo2C–(Co,Ni) system,” *Int. J. Refract. Met. Hard Mater.*, vol. 27, no. 1, pp. 9–13, 2009.

[26]Z. Liu, Q. Han, and J. Li, “A developed method for producing in situ TiC/Al composites by using quick preheating treatment and ultrasonic vibration,” *Compos. Part B Eng.*, vol. 43, no. 5, pp. 2429–2433, 2012

[27]N. M. PARIKH and M. H. JR., “Cermets: II, Wettability and Microstructure Studies in Liquid-Phase Sintering,” *J. Am. Ceram. Soc.*, vol. 40, no. 9, pp. 315–320, 1957.

[28]F. Qi and S. Kang, “A study on microstructural changes in Ti(CN)–NbC–Ni cermets,” *Mater. Sci. Eng. A*, vol. 251, no. 1, pp. 276–285, 1998.

[29]J. Wang, Y. Liu, Y. Feng, J. Ye, and M. Tu, “Effect of NbC on the microstructure and sinterability of Ti(C0.7, N0.3)-based cermets,” *Int. J. Refract. Met. Hard Mater.*, vol. 27, no. 3, pp. 549–551, 2009.

[30]W. Wan, J. Xiong, M. Yang, Z. Guo, G. Dong, and C. Yi, “Effects of Cr3C2 addition on the corrosion behavior of Ti(C, N)-based cermets,” *Int. J. Refract. Met. Hard Mater.*, vol. 31, pp. 179–186, 2012.

[31]J. Kübarsepp, H. Reshetnyak, and H. Annuka, “Characterization of the serviceability of steel bonded hardmetals,” *Int. J. Refract. Met. Hard Mater.*, vol. 12, no. 6, pp. 341–348, 1993.

[32]I. Hussainova, “Effect of microstructure on the erosive wear of titanium carbide-based cermets,” *Wear*, vol. 255, no. 1, pp. 121–128, 2003.

[33]W. Wan, J. Xiong, M. Yang, Z. Guo, G. Dong, and C. Yi, “Effects of Cr3C2 addition on the corrosion behavior of Ti(C, N)-based cermets,” *Int. J. Refract. Met. Hard Mater.*, vol. 31, pp. 179–186, 2012.

[34]G. Levi, W. D. Kaplan, and M. Bamberger, “Structure refinement of titanium carbonitride ž TiCN /,” no. June, pp. 344–350, 1998.

[35]G. Levi, W. D. Kaplan, and M. Bamberger, “Structure refinement of titanium carbonitride ž TiCN /,” no. June, pp. 344–350, 1998

[36]Randall M. German “Powder Metallurgy and Particulate Materials Processing”, pp. 248-253.

[37]Mohamed N. Rahaman, “Sintering of Ceramics”, pp. 206-208.

[38]V. Viswanathan, T. Laha, K. Balani, A. Agarwal, and S. Seal, "Challenges and advances in nanocomposite processing techniques," *Mater. Sci. Eng. R Reports*, vol. 54, no. 5, pp. 121–285, 2006.

[39]B.V.M. Kumar, JR Kumar, B Basu, "Crater wear mechanisms of TiCN-Ni-WC cermets during dry machining," International Journal of Refractory Metals and Hard Materials, vol. 25, pp. 392-399, 2007.

[40]V. Viswanathan, T. Laha, K. Balani, A. Agarwal, and S. Seal, "Challenges and advances in nanocomposite processing techniques," *Mater. Sci. Eng. R Reports*, vol. 54, no. 5, pp. 121–285, 2006.

[41]L. Takacs, "Self-Sustaining Metal – Sulfur Reactions Induced by Ball Milling," *J. Mater.*, vol. 8, 2000.

[42]J. M. Córdoba, M. J. Sayagués, M. D. Alcalá, and F. J. Gotor, "Monophasic $Ti_{y}Nb_{1-y}C_{x}N_{1-x}$ nanopowders obtained at room temperature by MSR," *J. Mater. Chem.*, vol. 17, no. 7, pp. 650–653, 2007

[43]K. Yang, Q. Yang, and Y. F. Bao, "Formation of carbonitride precipitates in hardfacing alloy with niobium addition," *Rare Met.*, vol. 32, no. 1, pp. 52–56, 2013.

[44]Y. Peng *et al.*, "Effect of SiC nano-whisker addition on TiCN-based cermets prepared by spark plasma sintering," *Int. J. Refract. Met. Hard Mater.*, vol. 34, pp. 36–40, 2012.

[45]Y. Ding and L. JW, "Study on the SiC whisker toughening Ti(C, N)-based cermet composites," *Powder Met. Technol*, vol. 25, no. 256, p. 9, 2007.

[46] H. Zhang, J. Yi, and S. Gu, "Mechanical properties and microstructure of Ti(C,N) based cermets reinforced by nano-Si3N4 particles," *Int. J. Refract. Met. Hard Mater.*, vol. 29, no. 2, pp. 158–162, 2011

*[47]*S. Zhang and S. C. Tam, "Mechanical alloying of a TiC□TiN ceramic system," *J. Mater. Process. Technol.*, vol. 67, no. 1, pp. 112–116, 1997.

[48]Y. Jin, Y. Liu, Y. Wang, and J. Ye, "Synthesis of ultrafine (Ti, W, Mo, V)(C, N)–Ni composite powders by low-energy milling and subsequent carbothermal reduction–nitridation reaction," *Journal of Alloys and Compounds*, vol. 486, no. 1. pp. L34–L36, 2009.

[49]P. Feng, W. Xiong, H. Zheng, Y. LX, and Y. Xia, "Spark plasma sintering properties of ultrafine Ti(C, N)-based Cermet," *J Wuhan Univ Technol*, vol. 19, pp. 69–72, 2004.

[50]Y. Dike, Z. Houan2, Y. Jiyong1, and T. Siwen, "Study on Preparation and Microwave Sintering

[51]Process of Ultra-fine TiCN Matrix Cermet," *Hot Work. Technol.*, vol. 20, 2010.

[52]V. Verma, "Ti(CN) based cermet system for the improved wear and machining performance", PhD Thesis, 2017